Simulating Planet Formation Around M-Type Dwarf Stars

Chris Bonadonna

Introduction:

Planets and Extra Solar Planets

Most people are familiar with the planets within our own solar system: Mercury, Venus, Earth, Mars, Jupiter, Saturn, Uranus, and Neptune. In general, a planet is an object that is gravitationally bound and supported from collapsing gravitationally by either the Coulomb pressure or electron degeneracy pressure. The difference between planets and stars is that planets do not sustain any nuclear fusion (Seager and Lissauer, 2010). This places an upper limit on the masses of planets at around 13 times the mass of Jupiter; above that mass limit planets typically fuse deuterium for a portion of their lifetime and are classified as brown dwarfs, which are the smallest non-planetary bodies (Hubbard et al. 2002). There isn't a clear lower limit on planetary mass, and that is a matter of some debate still. Nevertheless, applying this definition loosely should give a general idea of what a planet is.

Planets can be broadly classified into two categories: terrestrial planets and giant planets. A terrestrial planet is typically composed primarily of rock and metal, and they are supported from collapsing gravitationally by Coulomb pressure. They additionally must have a surface defined by the radial limit of a solid or liquid interior. The masses of terrestrial planets can range up to 5-10 earth masses. Above this mass, the planet is large enough to accrete substantial amounts of ice and gas onto its surface and become a giant planet. Giant planets are defined by having large gas envelopes. There are two broad classes of giant planets, both of which we observe in our solar system. Ice giant planets are defined by their substantial quantity of ice relative to their mass (~15% or higher). Gas giant planets are almost entirely gaseous, likely with small cores, and can be represented by polytropic equations of state. In our solar system Jupiter and Saturn are gas giant planets, and Uranus and Neptune are ice giant planets (Levine et al. 2006). Within each of these large classes, there are various subtypes, many of which are not found in our own solar system.

Extra solar planets, or exoplanets, are planets that orbit stars other than the Sun. These planets occur in a wide range of planetary systems, some similar to our own and others entirely different. As of March 8, 2015, 1523 of these planets have been found and confirmed, and an additional 3303 are unconfirmed (Han et al. 2014). These exoplanets are typically categorized based on size and semi-major axis, the distance from their star. The size of the planet, including both the mass and radius, can be used to determine the composition of the planet.

The criteria of mass and semi-major axis are also important for helping to identify other habitable worlds. Planets that we consider habitable will have atmospheres and pressures somewhat similar to earth, and they will be inside the habitable zone. The habitable zone is the area around a star where the temperature is in the proper range for liquid water, which is considered a likely requirement for life. This is primarily determined by the semi-major axis of the planet, as the temperatures of the planets are largely dictated by how far they are from their host star (Segura and Kaltenegger 2009). Finding these potentially habitable worlds, and

therefore possibly other life, is a stated goal of NASA and a driving force behind missions such as Kepler[1].

Exoplanet Detection

There are several methods that can be used to detect extra solar planets. These include timing pulsars and pulsating stars, radial velocity measurements, astrometry, transit photometry, transit timing variation, microlensing, and direct imaging. Of these, astrometry, transit timing variations, and direct imaging are less useful for initial detection of exoplanets. Detection by transit photometry (which I will refer to simply as detection by transits) is the most commonly used technique, and microlensing, radial velocity measurements, timing pulsars and pulsating stars, and direct imaging are all important for various reasons. As the transits method is by far the most prevalent, I will only go into detail in describing this particular method.

The transit method of detecting exoplanets has been the most commonly used, and it is responsible, in large part, for the success of the Kepler space mission. The basic principle behind exoplanet detection via transits is that the amount of light a star gives off can be measured fairly accurately, and when a planet passes in front of the star, the flux decreases. These changes in flux cause dips in the light curves that we observe from the stars and inform us that the planet is present. This method is most sensitive to planets with large radii and those that are closer to their host star. This leads to a bias towards large planets with short semi-major axes, unfortunately. Analysis of the photometric light curves is all that is needed to determine the presence of the planet, making it an extremely convenient method for finding exoplanets.

The majority of the planets that have been detected so far were found through the CoRoT (Convection, Rotation and Transits) and Kepler missions. Kepler is a .95-meter telescope that was launched by NASA in 2009. It observes the light curves of stars and enables the detection of exoplanets through dips or variations in the light curves that would indicate a transiting object (Lissauer, Dawson, and Tremaine 2014; Borucki et al. 2010). CoRoT was launched December 27, 2006. It has a 27-centimeter aperture and four 2048 x 2048 pixel CCDs, two of which are devoted to planet finding. As with Kepler, the exoplanets are found using the light curves of the stars that CoRoT observes (Aigrain et al. 2007). Given the large number of exoplanets found so far it becomes clear that there is a huge population of these objects in our galaxy, and it is important to study exoplanets and their related processes.

Beyond the planets that have already been identified around other stars, it is expected that many more, along with better characterizations, will be found in the near future. This will be done through missions such as the Transiting Exoplanet Survey Satellite Mission (TESS), the Wide Field Infrared Space Telescope (WFIRST), and the James Webb Space Telescope (JWST). TESS has an anticipated launch date in 2017 as part of an Astrophysics Explorer mission selected by NASA. It will look for planets via transits (Ricker et al. 2014). WFIRST will use microlensing to determine the demographics of exoplanets, and it will be capable of direct imaging of giant

planets and debris disks using a coronagraph (Spergel, Gehrels, et al. 2013). WFIRST would have a 2.4-meter aperture if approved and would likely launch in the early 2020s (Redy 2014). JWST will be able to perform direct imaging of gas giants, characterize atmospheres, and observe transits. It is scheduled to launch in October 2018[2]. Not only have we already found a substantial number of exoplanets, there will also be more and better exoplanet data available in the near future due to these missions.

For the planets that we have found, we can use their semimajor axis and mass to determine some of their important properties. Of particular interest to NASA and some planetary scientists is the question of habitability. As mentioned previously, there are a variety of conditions that must be fulfilled to have a habitable planet, but chief among them is temperature. Temperature of a planet is also based on a plethora of variables, but the most relevant of these is the semimajor axis. For this reason, we can use the exoplanet data to determine rough estimates on the temperature of the planets. This has been done for each of the planets that have been found thus far, and they have been arranged in a table broken up based on temperature (habitability) and demographics (mass). This is a useful way of depicting the planets to see which types are habitable and which are the most common that we've found so far. Note that, due to biases in exoplanet detection methods, this is not necessarily a perfect representation of all exoplanets, only ones that we have discovered.

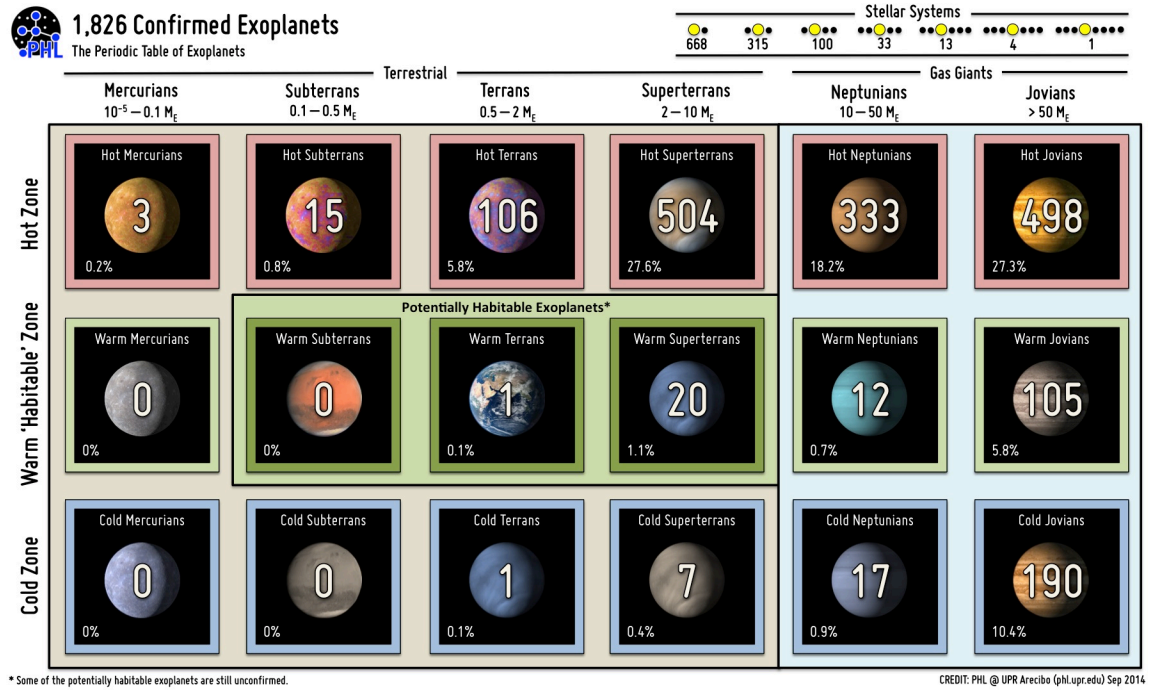

This second table includes all of the exoplanet candidates, not only those that have been confirmed by multiple observations.

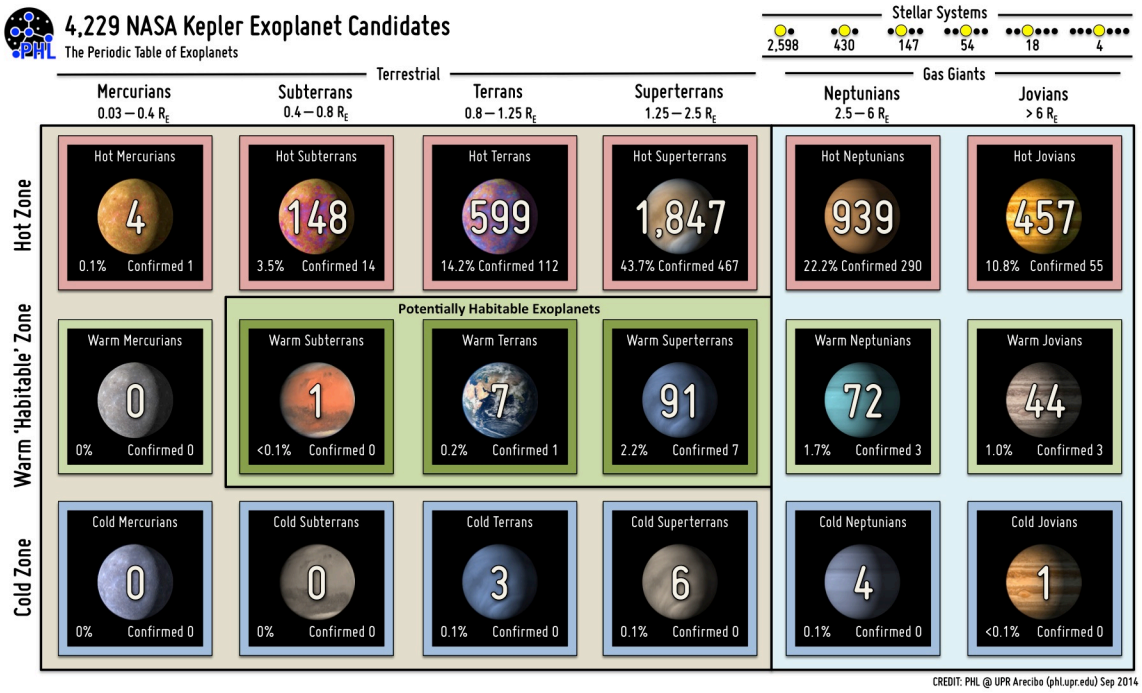

[3]Note: Both of these images are current as of September 1, 2014.

Planetary Formation

Now that it has been firmly established that there are other planets outside of our solar system, we need to explore how they came to be. There are two primary theories that have been proposed to describe planetary formation. Both theories begin with the assumption of a star surrounded by a giant disk of gas and dust (mostly gas), otherwise known as a protoplanetary disk. One theory is based on Gravitational Instability to account for gas giant planet formation. The other theory is based on an accretionary model. There is no true consensus as to which model is correct yet, although the accretionary model is heavily favored. The data from the JUNO mission will give us more information about the core of Jupiter and some insight into which model is likely to be more accurate for our solar system[4].

Formation of terrestrial planets can be the same in both the Gravitational Instability model and the core accretion model. The basic premise behind terrestrial planet formation is that dust particles will stick together and form larger particles, which will evolve collisionally to form larger particles and eventually planets. Dust grains stick together through electrostatic forces when they collide at low speeds. When the grains reach ~1 meter in size, electrostatic forces are insufficient to continue holding the particles together, and they have insufficient mass for gravitational forces to hold them together through collisions. This problem is often referred to as the "meter-sized barrier." This is one of the biggest problems in the accretion model, although some models use disk turbulence to solve it. Once the solid bodies reach 1 to 1000 kilometers in size, they are considered planetesimals. Once planetesimals reach this size, they have sufficient gravitational fields to pull in solid matter near their path instead of only that which is directly in the path that

they sweep out in the disk. As planetesimals combine together, the largest of them grow much more quickly than smaller ones, a process called runaway growth. Eventually, the disk reaches a state where regions of the disk are dominated by these large solid bodies, which are classified as planetary embryos. The process of forming planetary embryos from planetesimals takes between 10^5 to 10^6 years. These planetary embryos evolve collisionally with each other and planetesimals to form planets, which can grow large enough to accrete atmospheres. It takes on the order of 10^7 to 10^8 years to form planets from planetary embryos (Morbidelli et al. 2012). The accretionary model of gas giant planet formation is similar to this process.

The planetary formation model favored by a large portion of the community is the accretionary model, and the process is very similar to the formation process for terrestrial planets. All of the steps up until planetary embryos are roughly the same, albeit on a shorter time scale. To form cores of giant planets, embryos evolve collisionally with each other and planetesimals until they grow massive enough to pull in enough gas to begin runaway gas accretion. The mass at which this occurs is 5-10 earth masses (Hubickyj et al., 2005). Runaway gas accretion pulls in gas from the disk until it runs out of gas to accrete. This depletion of gas near the planet can be caused by photoevaporation in that region or a gap opening in the disk around the planet. The gap in the disk is caused simply by the planet having pulled in enough of the gas from the protoplanetary disk. The resulting body is what we consider a giant planet. Photoevaporation typically occurs after a few million years, so gas giant planets must be formed before then (Chambers, 2010), and this is why the shorter time scales are needed for giant planet formation compared to terrestrial planet formation.

The gravitational instability model championed by Boss seeks to provide an alternative explanation for gas giant planet formation and follows accretion principles for terrestrial planets. The fundamental idea behind the model is based on the idea that fluctuations in the protoplanetary disk could give rise to areas of extremely high density. These high-density areas would then have enough mass and density to stick together through their own self-gravity, leading to planetary formation. This mode of formation would lead to much shorter time scales for planet formation than those in the accretionary model. It would also lead to much lower solid core masses in giant planets (Boss, 1997). It should be noted that it is also possible for earthlike planets to form through gravitational instability as well (Boss, 2006). Note that this work will primarily be concerned with the accretionary model.

The Purpose of this Thesis

The purpose of this thesis is to investigate the types of planetary systems we should expect to find around M-type dwarf stars. The reason that this particular class of systems is important to investigate is due to the fact that we should be finding an increasingly greater number of them in the near future. As our technology, and thus detection capabilities, improve finding lower massed planets and planets around lower mass stars becomes increasingly likely. Additionally,

there is a marked bias towards examining systems with stars similar to our own (Endl et al., 2006). This makes these lower mass stars an excellent candidate to investigate to determine the characteristics of their planetary systems.

The way that we will be determining what planetary systems should look like around these stars is by simulating their formation from a protoplanetary disk. I'll go into greater detail about the process and parameters for the simulations in the methods section. I'll then analyze the resultant data in a results section and discuss the relevancy of the results. Specifically, I'll be investigating claims that M-dwarfs should have lower numbers of Jupiter-like planets (Johnson and Apps, 2009; Laughlin 2004). There have been some previous investigations into M-dwarf systems, such as those done in Ogihara and Ida (2009), but those tend to have a low number of high-resolution simulations. This work does the opposite by performing a large number of low-resolution simulations testing several sets of parameters. The purpose of this choice is to create a sample from which meaningful statistics can be computed and more general conclusions can be drawn. Throughout this thesis I'll be using the core accretion model to investigate the characteristics of these planetary systems.

Methods:

The Symplectic Integrator

I used the program SyMBA from the Swifter software package, written by David E. Kaufmann. The Swifter package is based on the Swift software package written by Hal Levison and Martin Duncan. The program SyMBA takes in several files that specify parameters such as particle masses, particle radii, particle semimajor axes, particle velocities, and runtime, among many others. It then uses this information to integrate the set of mutually gravitationally interacting masses. When particles collide, they are merged, and once particles travel too far away from the central mass (the star), they are discarded. In this way, the program takes a large suite of masses and simulates planetary formation through the collisional evolution of the particles.

It is possible to implement more advanced interactions within the program by writing additional code for the software. These interactions can lead to the inclusion of hit-and-run collisions and partial mergers. They can also create effective forces due to the gas in the disk. The inclusion of additional collision types isn't necessary, as no collisions result in a net loss of mass, and the primary effect of hit-and-run collisions would be to increase the time it takes for the disk to finish interacting with itself (Chambers, 2013). Disk forces can increase the accretion rate for bodies in the disk (Kenyon and Bromley, 2013), and they can damp eccentricities (Ogihara and Ida, 2009). They can also influence the interactions for large numbers of particles (high-resolution simulations) through dynamical friction (Raymond et al., 2006). The work in this thesis isn't concerned with the time-scales involved with the formation of planets, which enables the simplifying assumption of purely merging collisions. Not being concerned about the time-scales, in conjunction with the fact that the simulations are low-resolution, makes it possible to also ignore the

external disk forces. Examples of simulations that account for these additional complexities can be found in papers such as Tanaka and Ward (2004). Essentially, neglecting these factors is possible due to these simulations being low resolution, and the time-scales for planet formation in these simulations should not be taken as representative for realistic scenarios.

Making the Disk

The bulk of the programming for this project lay in writing a program to construct files with planetesimals for a protoplanetary disk. There have been several different ways different researchers have gone about setting up their disks, so here I'll delineate my own methodology. Disks have been made using varying masses for planetesimals (Raymond et al., 2006) and uniformly massed planetesimals (Raymond et al., 2004). I opted for a disk that used uniform masses so that I could use a more elegant algorithm than something along the lines of binning. Essentially, when using constant masses for the planetesimals, you can write a formula that takes a random number between 0 and 1 and places the mass according to a specified distribution. This is done by inverting the cumulative distribution function for the mass profile of the distribution and then using the random number that was generated. Starting with the surface mass density profile, Σ:

$$\Sigma = cr^{-\alpha} \tag{1}$$

Where c is a constant scaling factor and α is the power that the distribution follows. The value of α can vary somewhat, although the most common value is $3/2$. To obtain the cumulative distribution function (in this case the integrated mass function), we integrate over the area of the disk. Representing the cumulative distribution function as y(r):

$$y(r) = \int \Sigma dA \tag{2}$$

As the disk is idealized as a circle in the simulations, we can substitute:

$$y(r) = \int cr^{-\alpha} 2\pi r dr \tag{3}$$

Performing the integral yields:

$$y(r) = \frac{2\pi c}{2-\alpha} r^{2-\alpha} \tag{4}$$

evaluated over the radius of the disk. Now we invert the function to obtain r as a function of y, our random number between 0 and 1:

$$r = \left(\frac{2-\alpha}{2\pi c}\right)^{\frac{1}{2-\alpha}} y^{\frac{1}{2-\alpha}} \tag{5}$$

So to obtain a random radius fitting a certain surface mass density, we can simply pick a random number between 0 and 1 (using a random number generator) and substitute that in for y after we normalize the function. Fortunately, normalizing the function is nearly trivial, and it doesn't require knowledge of the values of c or α. Because the range of y is [0,1), the range of:

$$y^{\frac{1}{2-\alpha}} \tag{6}$$

is also [0, 1). This means that, for the range of r to be [r_{min}, r_{max}), the equation becomes:

$$r = [r_{max} - r_{min}] y^{\frac{1}{2-\alpha}} + r_{min} \tag{7}$$

This is the closed form solution that can be applied to any surface mass density profile that is invertible. I varied the value of α for some of the simulations, which is why the derivation was done here with the general form.

Now that we've determined the formula we'll use to determine the radii of planetesimals randomly, we can establish the process for making the disk. The important parameters that can be varied are: star mass, r_{min}, r_{max}, gas-to-solid ratio, disk-to-star mass ratio, planetesimal number, and planetesimal density. The program starts by calculating the mass of solids in the protoplanetary disk using the fairly straightforward formula:

$$M_{Disk} = M_* \frac{(Disk\ to\ star\ mass\ ratio)}{(gas\ to\ solid\ ratio)} \tag{8}$$

Following this, the mass of each planetesimal can be found by dividing the disk mass by the planetesimal number. The program then determines the radius of the planetesimals using the standard formula found by solving the definition of density of a sphere for radius:

$$r = \left(\frac{3M_p}{4\pi\rho}\right)^{1/3} \tag{9}$$

where M_p is the mass of the planetesimal and ρ is its density. Following this, the program calculates the part of the hill radius that will be the same for each planetesimal, given by:

$$\frac{r_{Hill}}{a} = \left(\frac{M_p}{3M_*}\right)^{1/3} \tag{10}$$

where a is the semimajor axis of the particle, which varies from particle to particle. The Hill radius represents the radius within which the planetesimal will dominate the attraction of matter. This value will be used later to calculate the hill radius of each planetesimal after their semimajor axes have been determined.

So far, all that's been done is the pre-processing for the calculations that will be carried out to create the disk. Now the program loops through for the number of planetesimals that need to be created and picks a semimajor axis according to formula (7). It then uses the semimajor axis to calculate the Hill radius:

$$r_{Hill} = a\left(\frac{M_p}{3M_*}\right)^{1/3} \tag{11}$$

where, as before, a is the semimajor axis. The program then picks a random angle between 0 and 2π and calculates the x and y positions using standard sine and cosine functions. After this the orbital velocity is calculated based on centripetal motion:

$$|v| = \left(\frac{GM_*}{a}\right)^{1/2} \tag{12}$$

This is then split up into its components based on the angle used for the x and y positions. Finally, the position is checked against all previously placed planetesimals to ensure that it is not within another planetesimal's Hill sphere. If it is within another planetesimal's Hill sphere, a new semimajor axis is chosen, and the process is repeated. Note that, in these calculations, there is no inclination, so the positions and motion are restricted to a plane. This is not an uncommon practice (Chambers and Wetherill, 1998), as it lowers computation time and planetary disks are nearly flat anyway. Using an inclination of zero does distort the time-scales, but, as mentioned earlier, we won't be examining the time-scales here, so this is acceptable. Furthermore, additional accretion criteria do not lead to substantial differences, so the choices of near perfect conditions are acceptable (Kokubo and Genda, 2010). Once all of the planetesimals have been created, the disk is complete, and it can be fed into the program. The code (in python) used to create the disk can be found in Appendix 1.

Parameters

Here I will discuss the choices that were made for each of the parameters that can be varied. These parameters are: star mass, r_{min}, r_{max}, gas-to-solid ratio, disk-to-star mass ratio, surface mass density dependence (α), planetesimal number,

and planetesimal density. Some of these parameters were kept constant for each set of simulations while others were varied deliberately.

The parameters that were kept constant were the stellar mass, r_{min}, r_{max}, gas-to-solid ratio, planetesimal number, and planetesimal density. Although the planetesimal density is largely unimportant (Kokubo et al., 2006), I attempted to pick a realistic density for the planetesimals. I chose to use a density of 3 g/cm^3 both because it is the density of rock and because it is a density that has been used by other researchers (Raymond et al., 2005). Similarly, the actual values for gas-to-solid ratio and disk-to-star mass ratio aren't important by themselves; they are only relevant in their contribution to the mass of solids in the disk. Again, realistic values were selected, in this case to obtain a realistic mass of solids in the disk. I chose a gas-to-solids ratio of 70:1 based on Laughlin et al. (2004). This ratio is largely unconstrained, and it has been suggested that it could be as high as 100:1 (Roberge and Kamp, 2010). The stellar mass selected, one third of the mass of the sun, is roughly in the middle of the M-dwarf range (Kalteneggar and Traub, 2009). A small gap of .05 AU was left to make r_{min} non-zero, as protoplanetary disks typically have a gap between their inner edge and their host star (Ogihara and Ida, 2009). The outer radius, r_{max}, was chosen to be 30 AU. This radius was chosen due to the suggestion that some protoplanetary disks are 10's of AU (Roberge and Kamp, 2010), the most distant planet in our solar system, and the work of Alibert et al. (2011). The simulations used 1000 planetesimals due to run-time constraints and a desire to avoid dynamical friction that would require the inclusion of disk forces. The total mass of the embryos is also the only relevant factor when considering planetesimal mass and number (Raymond et al., 2014), so the low-resolution simulations that result from using 1000 planetesimals are still valid. Each simulation was run for 100 million years, although this does not necessarily relate well to realistic times. Note that the simulations will be good for finding earth-sized and larger planets, but should not be taken as indicative for finding smaller planets such as mercury due to the large planetesimal size.

The parameters that were varied between simulations were the total disk mass (thus varying the mass of solids in the disk) and the surface mass density profile. Andrews et al. (2013) found disks to have masses between .2% and .6% of their host stars mass. Beckwith et al. (1990) found an average disk mass of 2% of star mass, and Andrews and Williams (2005) found an average disk mass of .5% the stellar mass, with an upper limit of 20% of the stellar mass. Clearly the values are very unconstrained. I selected a disk mass of 2% of the star's mass as the "standard" case. I also tested disks with masses of .5% of the star's mass for a lighter case and 10% of the star's mass for the heavier case. For the surface mass density profile, a dependence of $r^{-3/2}$ is typically used (Roberge and Kamp, 2010; Ogihara and Ida, 2009). Despite this, it has been suggested that shallower profiles are also valid, down to a r^{-1} dependence (Raymond et al., 2007; Raymond et al., 2009). For this reason, I tested surface mass densities with a radial dependency of r^{-1} and $r^{-5/4}$ in addition to the standard $r^{-3/2}$. Five sets of 50 simulations were performed with the following combinations of radial dependence and disk mass, respectively: $r^{-3/2}$ and $.02M_*$, $r^{-3/2}$ and $.005M_*$, $r^{-3/2}$ and $.1M_*$, $r^{-5/4}$ and $.02M_*$, and r^{-1} and $.02M_*$.

For each of the sets of simulations it is also important to establish the entire formula for the surface mass density profile. Here I'll go over how to derive the constant in the formula in addition to the radial dependence. Recall that the general form for the surface mass density is:

$$\Sigma = cr^{-\alpha} \tag{13}$$

We can determine the value of c by working back from the cumulative mass distribution function. We know that the mass in the disk is given by:

$$M = \int \Sigma dA \tag{14}$$

Which, as computed previously in equation (4), results in:

$$M = \frac{2\pi c}{2-\alpha} r^{2-\alpha} \tag{15}$$

Solving this equation for the constant, c:

$$c = \frac{M(2-\alpha)}{2\pi r^{2-\alpha}} \tag{16}$$

Where we approximate r as $r_{max} - r_{min}$. Below are the parameters for each group of simulations in table form, including the full surface mass density profile (Note: The "standard" simulation is listed twice for comparison).

Parameters	Normal	Light	Heavy
Planetesimal Number	1000	1000	1000
Star Mass	$M_\odot/3$	$M_\odot/3$	$M_\odot/3$
Disk-to-Star Mass Ratio	.02	.005	.1
Gas-to-solid ratio	70	70	70
Mass of solids in Disk	$31.71 M_\oplus$	$7.93\ M_\oplus$	$158.5\ M_\oplus$
Planetesimal Density (g/cm^3)	3	3	3
Planetesimal Radius (km)	2,470	1,556	4,223
Min. Disk Radius (AU)	0.05	0.05	0.05
Max. Disk Radius (AU)	30	30	30
$\Sigma_{solids}\left(\frac{g}{cm^2}\right)$	$12.30\left(\frac{r}{1\ AU}\right)^{-3/2}$	$3.074\left(\frac{r}{1\ AU}\right)^{-3/2}$	$61.49\left(\frac{r}{1\ AU}\right)^{-3/2}$
$\Sigma\left(\frac{g}{cm^2}\right)$	$861\left(\frac{r}{1\ AU}\right)^{-3/2}$	$215\left(\frac{r}{1\ AU}\right)^{-3/2}$	$4300\left(\frac{r}{1\ AU}\right)^{-3/2}$

Parameters	Normal	Shallow	Shallower
Planetesimal Number	1000	1000	1000
Star Mass	$M_\odot/3$	$M_\odot/3$	$M_\odot/3$
Disk-to-Star Mass Ratio	.02	.02	.02
Gas-to-solid ratio	70	70	70
Mass of solids in Disk	$31.71 M_\oplus$	$31.71 M_\oplus$	$31.71 M_\oplus$
Planetesimal Density (g/cm^3)	3	3	3
Planetesimal Radius (km)	2,470	2,470	2,470
Min. Disk Radius (AU)	0.05	0.05	0.05
Max. Disk Radius (AU)	30	30	30
$\Sigma_{solids}\left(\frac{g}{cm^2}\right)$	$12.30\left(\frac{r}{1\ AU}\right)^{-3/2}$	$7.89\left(\frac{r}{1\ AU}\right)^{-5/4}$	$4.50\left(\frac{r}{1\ AU}\right)^{-1}$
$\Sigma\left(\frac{g}{cm^2}\right)$	$861\left(\frac{r}{1\ AU}\right)^{-3/2}$	$552\left(\frac{r}{1\ AU}\right)^{-5/4}$	$315\left(\frac{r}{1\ AU}\right)^{-1}$

The values for the surface mass density profiles were important to establish in order to determine how realistic the disk parameters are. A commonly used formulation for comparison is:

$$\Sigma = 1700\left(\frac{r}{1\ AU}\right)^{-3/2}\ \frac{g}{cm^2}$$

(Hayashi, 1981; Roberge and Kamp, 2011). From this, we can see that the value of Σ for our normal case is slightly lower than the value for the surface mass density often used canonically. This means that the results for these simulations should be fairly close to what we should typically expect, although it might be reasonable to expect slightly more mass in the disk. The light and heavy cases are intended to be extreme cases, and the values they yield for surface mass density seem to support this.

Results:

The Disks (Prior to simulation)

There are two main parts to the simulations involved with this project. First, the python script that was written had to produce the correct protoplanetary disks. After this, the disks were allowed to evolve according to their own self-gravitation. For this reason, as well as to verify the validity of the disk, we will analyze the results of the script. Essentially, here I will establish the veracity of the surface mass density profiles used. Below are graphs of the perfect mass distribution function

(exactly following the distribution for comparison) as well as an example from the normal case (the first simulation):

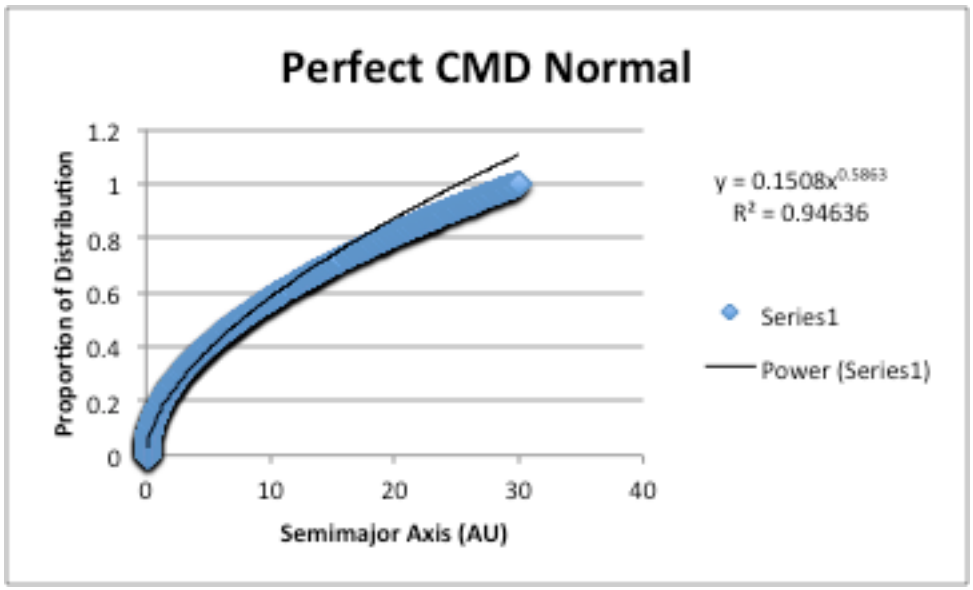

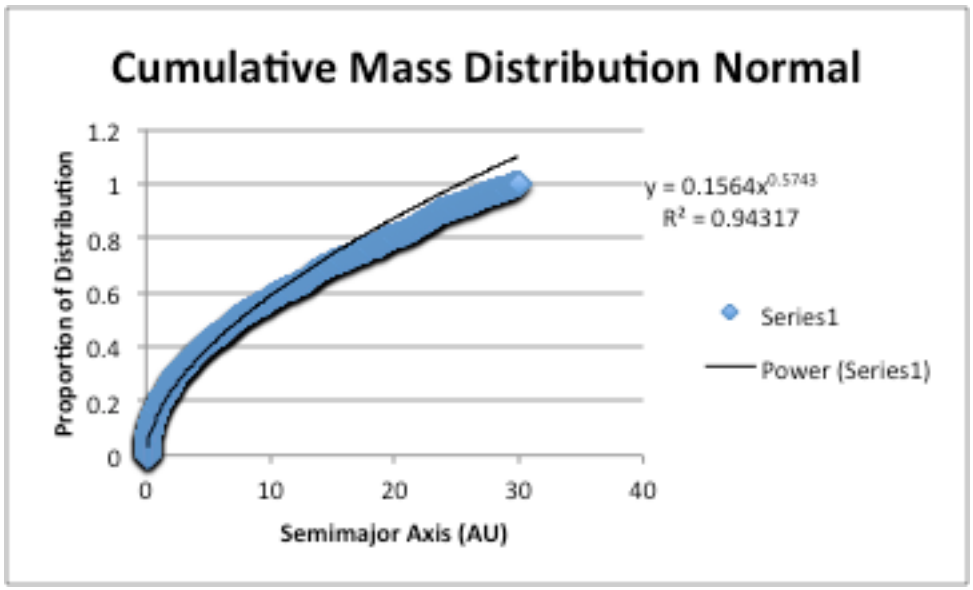

These two graphs are normalized to a total mass of one. The radial dependence of the top graph is exactly $r^{1/2}$, which is the theoretical radial dependence of a cumulative mass distribution function for a surface mass density distribution with a radial dependence of $r^{-3/2}$ (see equation 15). This is important to note because the equation generated for this graph has a radial dependence with a power of .5863. For comparison, the actual data yielded a radial dependence with a power of .5743, which is very close to the same value as in the ideal case. Additionally, the shapes of the curves in each of the graphs resemble each other closely with small deviations in the actual data as expected. Quantitatively, the standard deviation of the data from

the ideal case is .00780. This means that ~66% of the data points have a cumulative mass (their mass plus all mass interior to their own radius) within .780% of the idealized cumulative mass. Approximately 95% are with 1.560% of the idealized case. This distribution can be taken as indicative of all of the disks with the same radial dependence (the normal, heavy, and light cases) as the code used to generate them was identical in this regard. With this in mind, it is fairly clear that disks with the correct surface mass densities were generated for theses cases.

Now we'll perform the same analysis for the shallow (Σ proportional to $r^{-5/4}$) and shallower cases (Σ proportional to r^{-1}), respectively:

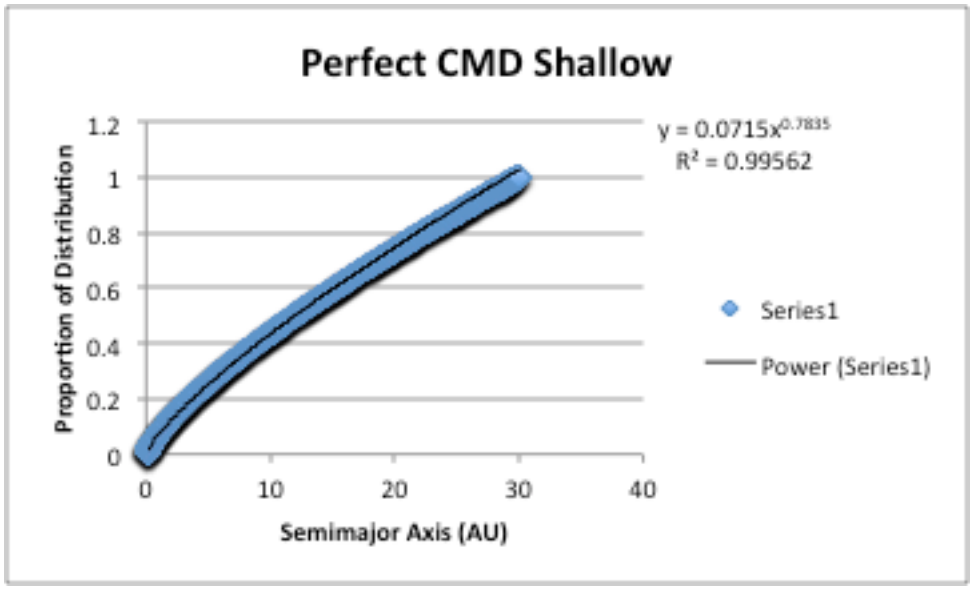

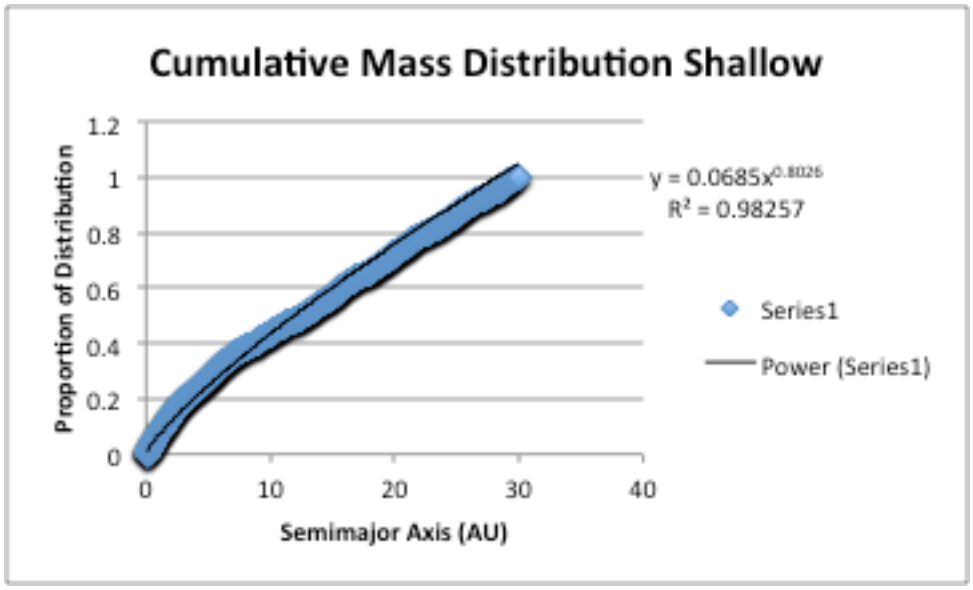

The radial dependence of the top graph, and thus the desired radial dependence of the bottom graph, is $r^{3/4}$. The equation generated in the perfect case has a radial dependence with a power of .7835. The data yielded an equation with a radial

dependence exponent of .8026. The standard deviation of the data from the idealized case (again, cumulative mass at each data point) is .0140. This means that the data is roughly twice as far from perfect as the normal case was, but it is still very clearly the correct distribution for the disk. This can be taken as indicative of the distribution for every disk in this suite of simulations because the code generating each is identical.

Finally, we perform the same analysis for the shallower case:

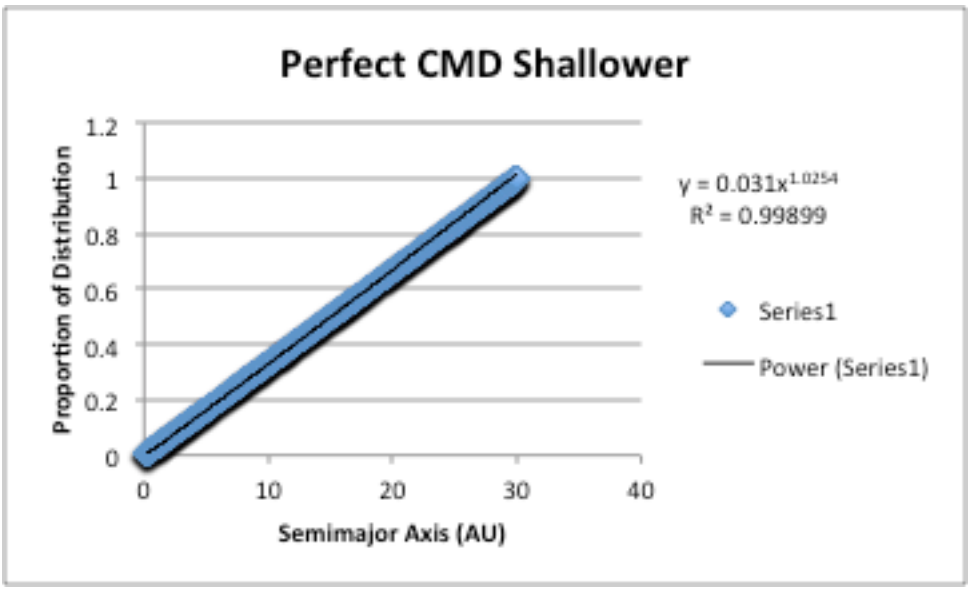

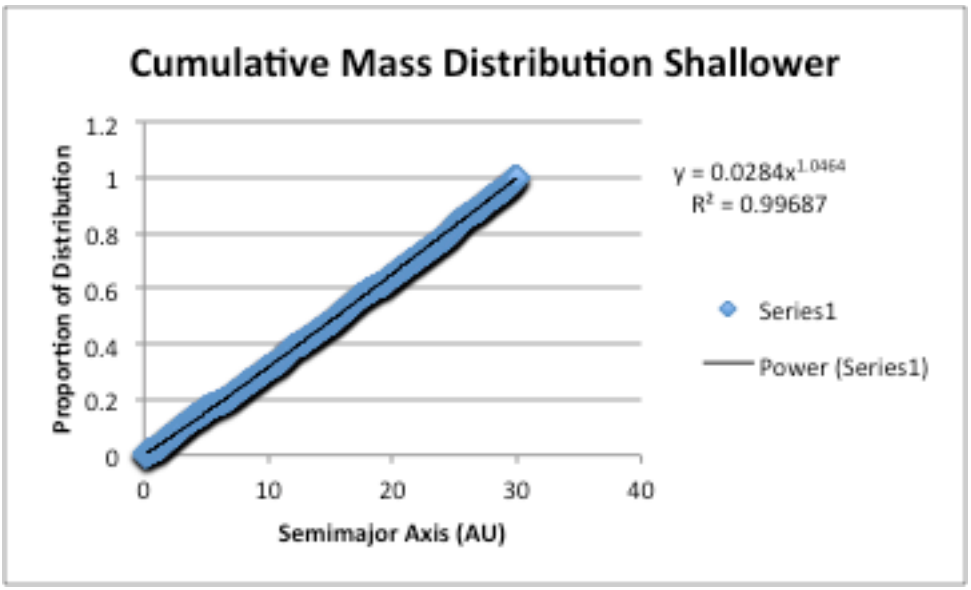

The radial dependence of the top graph, and thus the desired radial dependence of the bottom graph, is r^1. The equation generated in the perfect case has a radial dependence with a power of 1.0254. The data yielded an equation with a radial dependence exponent of 1.0464. The standard deviation of the data from the idealized case (again, cumulative mass at each data point) is .0150. As with the

shallow case, this data is slightly farther from the idealized case than the data was for the normal case, but it is still very clearly the correct distribution. Overall, each of the distributions can be shown to be exactly what was desired with the random deviations from the idealized cases.

Simulation Results

In this section, I will present the aggregated results of each set of simulations and discuss their meaning. I will also compare the results to predictions made by other researchers. Below is a table summarizing the results of the normal simulations. Note that masses are given in earth masses.

Normal	
Mean Mass	3.53
Median Mass	3.12
Mass Standard Deviation	2.82
Minimum Mass	0.032
Total Disk Mass	31.70
Average Remaining Mass	15.03
Planet Number	213
Mean Eccentricity	0.173
Eccentricity Standard Deviation	0.110
Number of Jupiters	62
Systems with Jupiters	47
Systems with Multiple Jupiters	15

In addition to this table, presented below are graphs representing the distribution of the planets in the simulations:

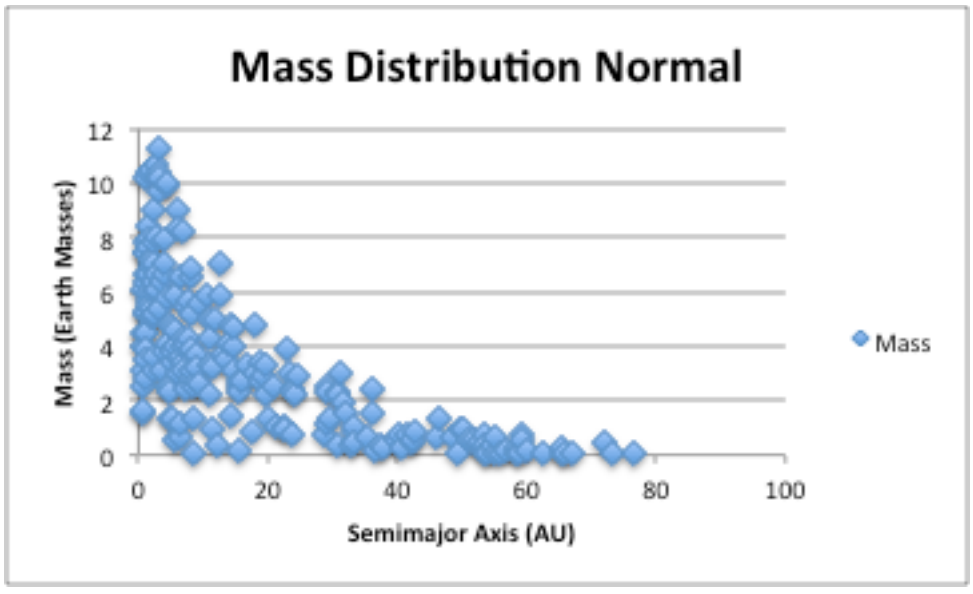

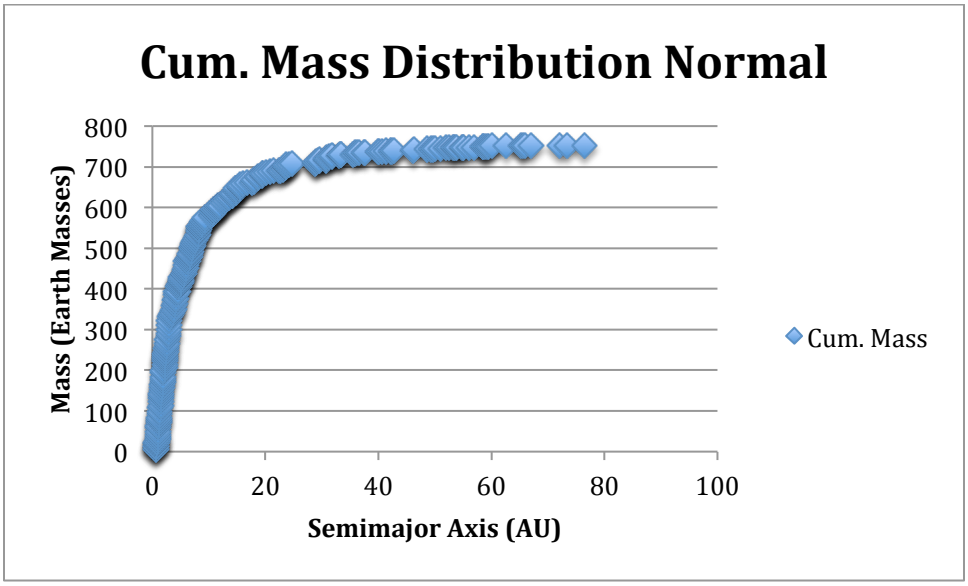

These graphs are primarily presented to show how the disks evolved over time from their original distributions. Below is a graph that should give an impression of the demographics of the planets that the simulations yielded:

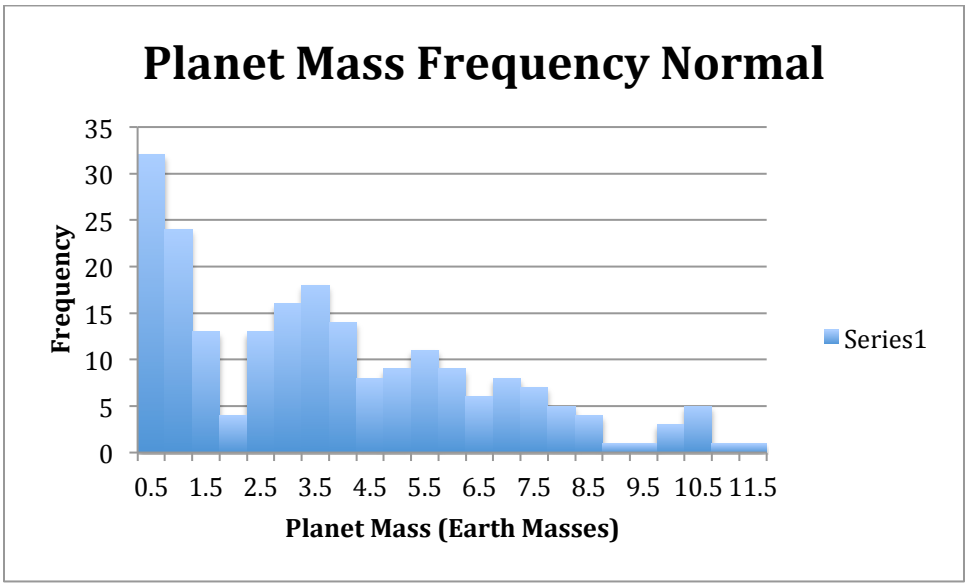

From the table and graphs, we see that the planets we should expect to find in this distribution have a peak between 2 and 4 earth masses, with an average planet mass of 3.53 earth masses. The median planet mass of 3.12 earth masses is also within this range. This means that, even around a lighter star, it is reasonable to expect heavier, super-earths around M-dwarfs than the terrestrial planets that we find in our own system. Additionally, objects with enough mass to start runaway gas

accretion were found in 47 out of the 50 simulations, and multiple bodies with this property were found in 17 out of the simulations. This suggests that it is likely, providing enough gas can accrete onto the planet, that Jupiter-like planets could form around M-dwarfs. The large number of potential Jupiters, and the large number of potential Jupiters with small semimajor axes, corroborates the work of Endl et al. (2006), who concluded that hot Jupiters are found around 1% to 2.5% of the time around M dwarfs. Additionally, Johnson (2014) found that there should be at least 1.5 planets per M dwarf, and Rivera et al. (2005) investigated a planetary system around an M-dwarf star and concluded that there were three planets around it. The results of this simulation showed just over 4 planets per M dwarf star, which is consistent with the findings of both of these papers. This is also consistent with the findings of Agnor et al. (1999), who found that 3 planets were most often formed in their simulations. While the eccentricity of the planets is typically very high in these simulations, this is most likely a result of the exclusion of gas in the disk simulations (Ogihara and Ida, 2009), so it should not be taken as a pertinent result of the simulations. Finally, the relatively high frequency of Jupiter cores in these simulations seems to support the finding that Giant planets can often form with a larger planet-to-star mass ratio than that of Jupiter and the Sun (Delfosse et al., 1998). From these simulations, we can be optimistic about the likelihood of finding plants, and especially Jupiter-like planets, around M-type dwarf stars.

Below we'll show similar data for the light case:

Light	
Mean Mass	0.95
Median Mass	0.89
Mass Standard Deviation	0.75
Minimum Mass	0.0080
Total Disk Mass	7.96
Average Remaining Mass	5.15
Planet Number	272
Mean Eccentricity	0.171
Eccentricity Standard Deviation	0.115
Number of Jupiters	0
Systems with Jupiters	0
Systems with Multiple Jupiters	0

The accompanying mass distribution graphs are:

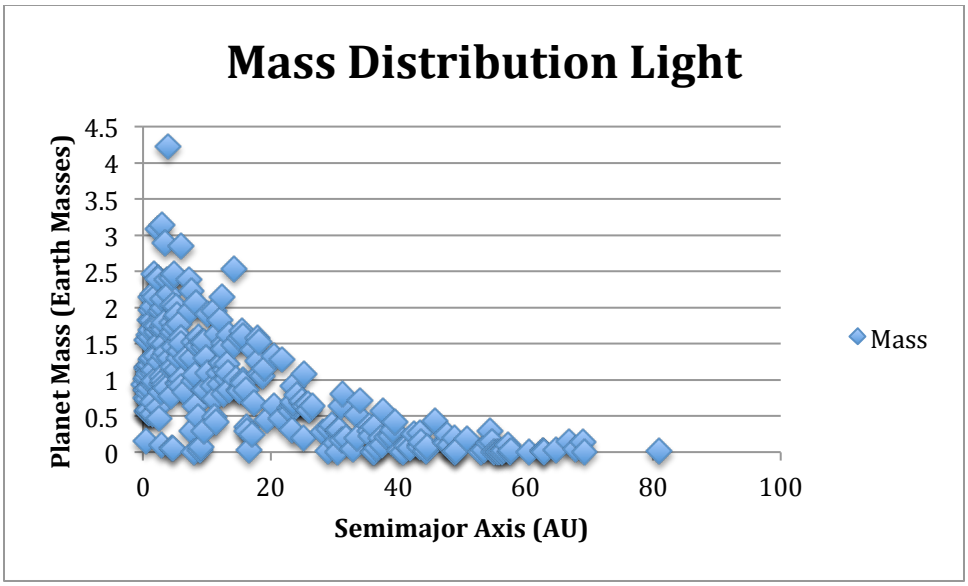

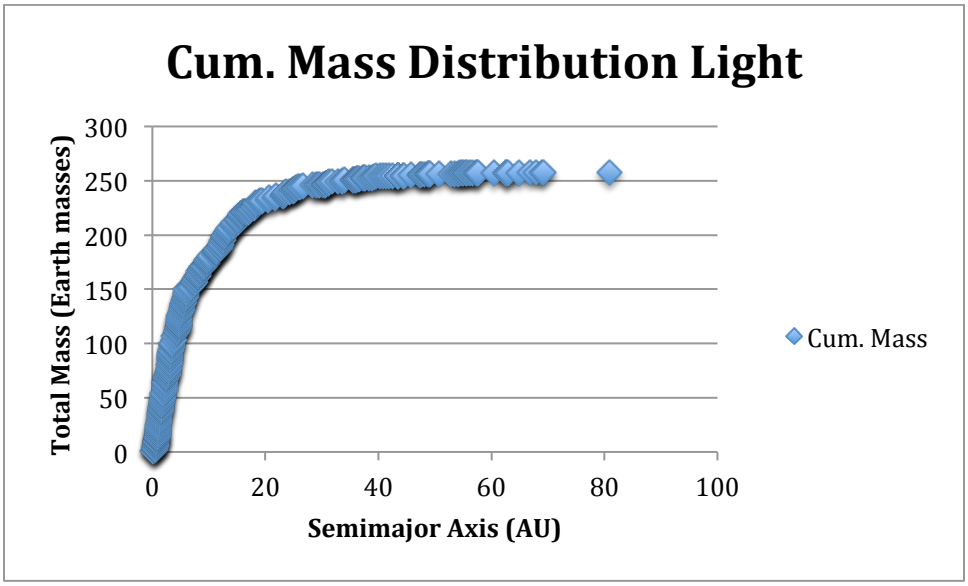

with the histogram with masses:

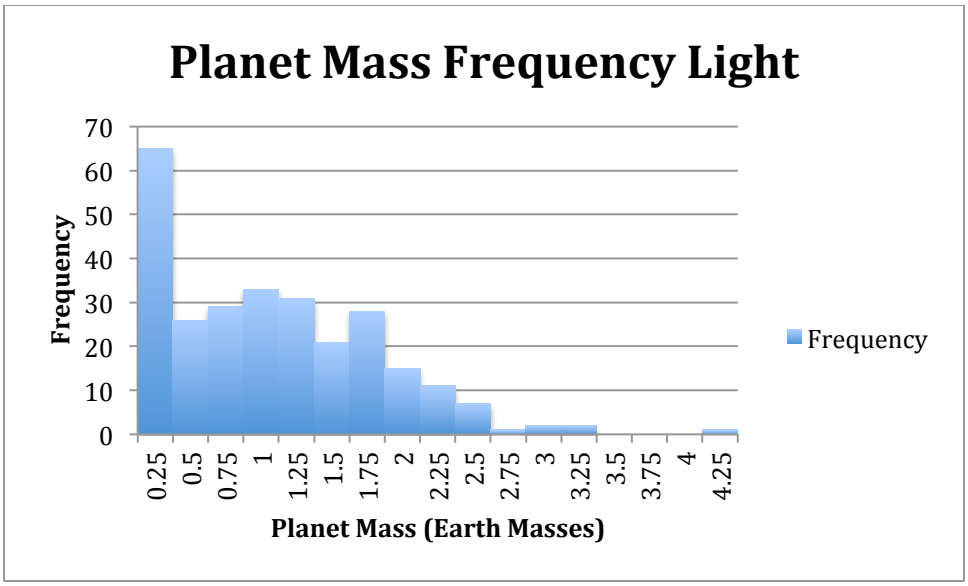

These simulations were intended to be the extreme case for a light disk mass. In this case, it seems that no Jupiters were formed, and the resultant disk was slightly shallower after it was allowed to interact with itself when compared to the normal case. There were a larger number of planets, perhaps due to the lighter masses of the planets preventing them from dominating as large areas of the disk, leading to fewer collisions. A greater proportion of the disk remained in the planets after the simulations completed, meaning less of the mass was ejected when compared to the normal case. The eccentricities were again high, but, as before, this should not be taken as an important finding due to the lack of damping factors. The most important conclusions we can draw from this set of simulations is that there was less development of the disk and there were lighter resultant planets to accompany the lighter disk mass.

Now we will present the findings for the heavy case in a similar manner:

Heavy	
Mean Mass	15.08
Median Mass	12.09
Mass Standard Deviation	13.01
Minimum Mass	0.159
Total Disk Mass	159.19
Average Remaining Mass	52.77
Planet Number	175
Mean Eccentricity	0.208
Eccentricity Standard Deviation	0.149
Number of Jupiters	120
Systems with Jupiters	50
Systems with Multiple Jupiters	48

The accompanying mass distribution graphs:

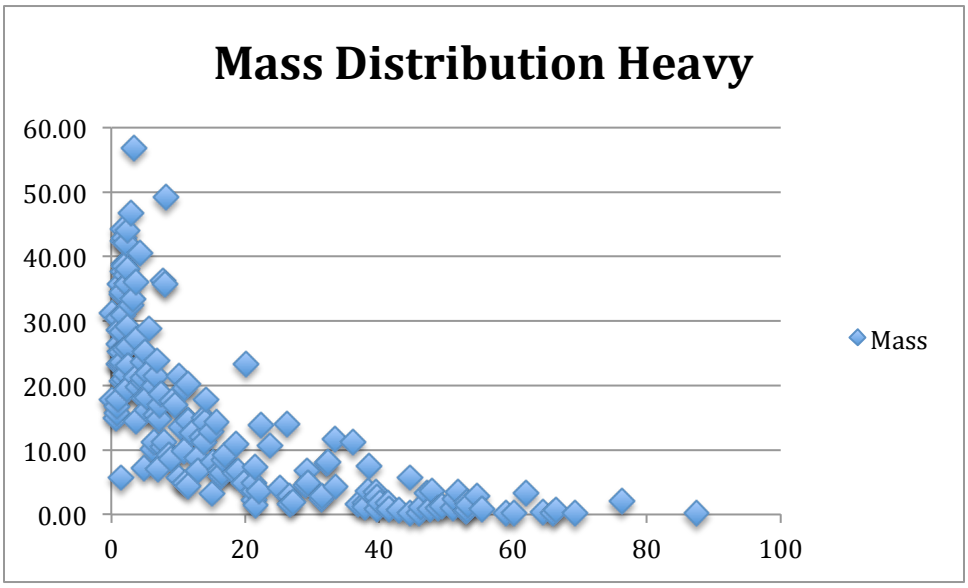

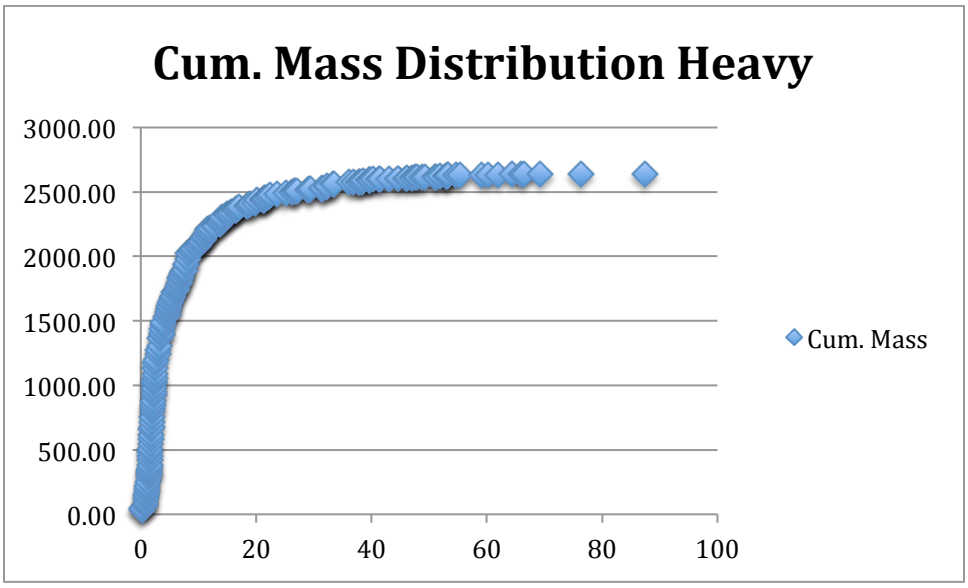

and the histogram of planet masses is:

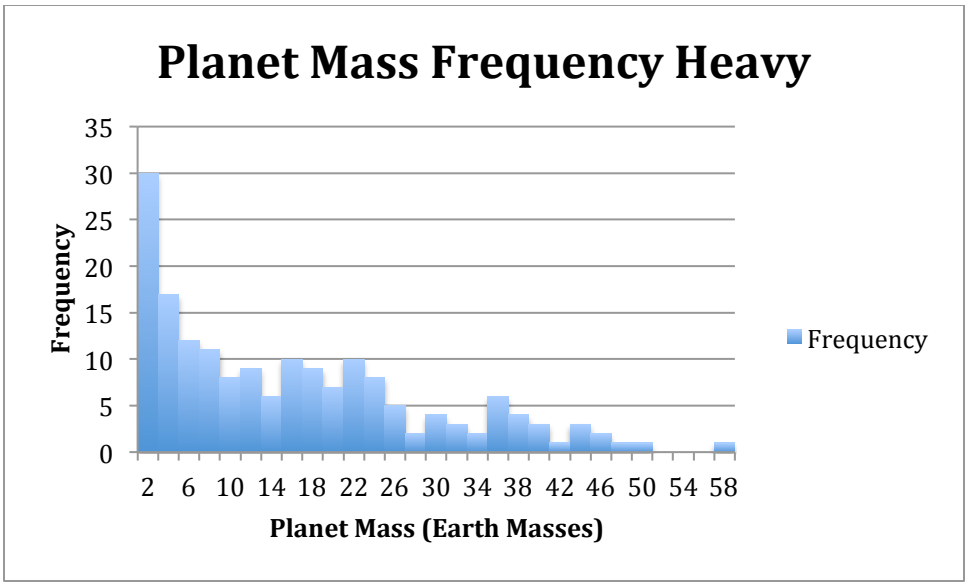

This set of simulations was intended to be the extreme case for heavier disks. Here, a Jupiter core was formed in every single simulation, and multiple Jupiter cores were formed in all but 2 of the 50 simulations. The typical planet masses were much higher than in the normal and light cases, and the mass distribution appears to be steeper than in either of those cases as well. The disk appears to have interacted more with itself, likely due to the higher planetary embryo masses dominating larger portions of the disk, than in the light and normal cases. Less of the mass from the initial disk remained in the planets at the conclusion of the simulations when compared to the normal case, meaning that a greater proportion of the disk mass was ejected. As before, the eccentricities are high, but, also as before, this should not be taken as an important finding. The important conclusions from the heavy simulations are that there are always Jupiters, the disk interacts more with itself, and the planets are heavier than in the other cases.

After seeing the results of the light, normal, and heavy simulations, several trends become immediately apparent. The masses of the planets found tend to increase with the masses of the disks. Similarly, the frequency of potential giant planets also scales with the mass of the disks. This supports the finding that the frequency of Jupiter-like planets increases linearly with stellar mass (Kennedy and Kenyon, 2008), as higher stellar masses correlates with higher disk masses. It does suggest, however, that disk mass might be the driving factor. To test this, it would be necessary to perform simulations with varying star masses but constant disk masses. In addition to this, it seems that the disk interacts more with itself as mass increases. This makes sense due to the runaway nature of accretion and how larger masses can dominate larger portions of the disk. Additionally, lighter disks tended to retain more of their initial disk mass, whereas heavier disks ejected more of their mass. Perhaps the most interesting result of the simulations is the trend that heavier disks led to steeper mass distributions of planets, despite starting with the same surface mass density profile. This is a result that would bear looking into more in the future.

Now that we've seen the results from varying the masses of the disks, we will examine the results for varying surface mass density profiles. Below we'll present the shallow case in the same manner as the other cases:

Shallow	
Mean Mass	3.83
Median Mass	3.59
Mass Standard Deviation	2.86
Minimum Mass	0.032
Total Disk Mass	31.84
Average Remaining Mass	16.39
Planet Number	214
Mean Eccentricity	0.176
Eccentricity Standard Deviation	0.100
Number of Jupiters	70
Systems with Jupiters	50
Systems with Multiple Jupiters	20

The accompanying mass distribution graphs:

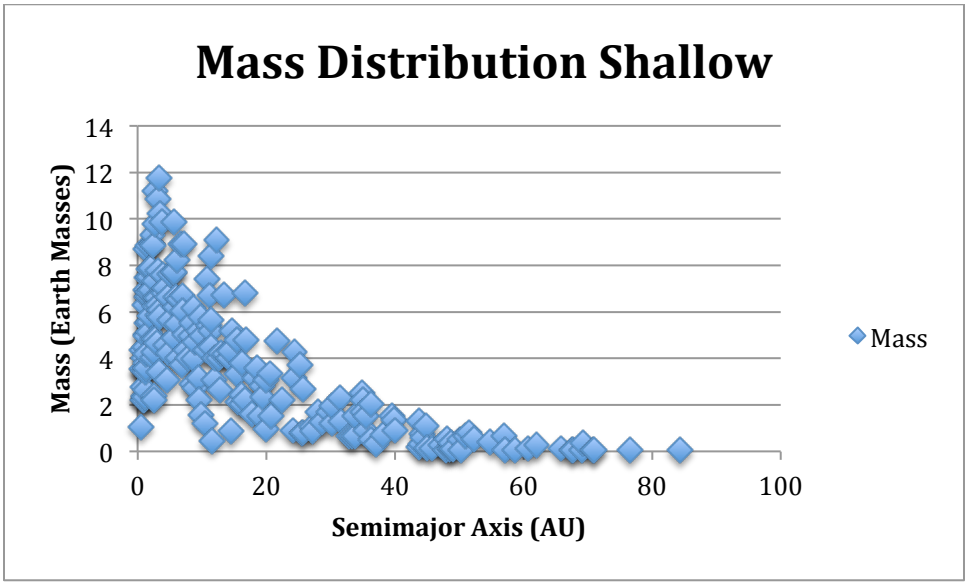

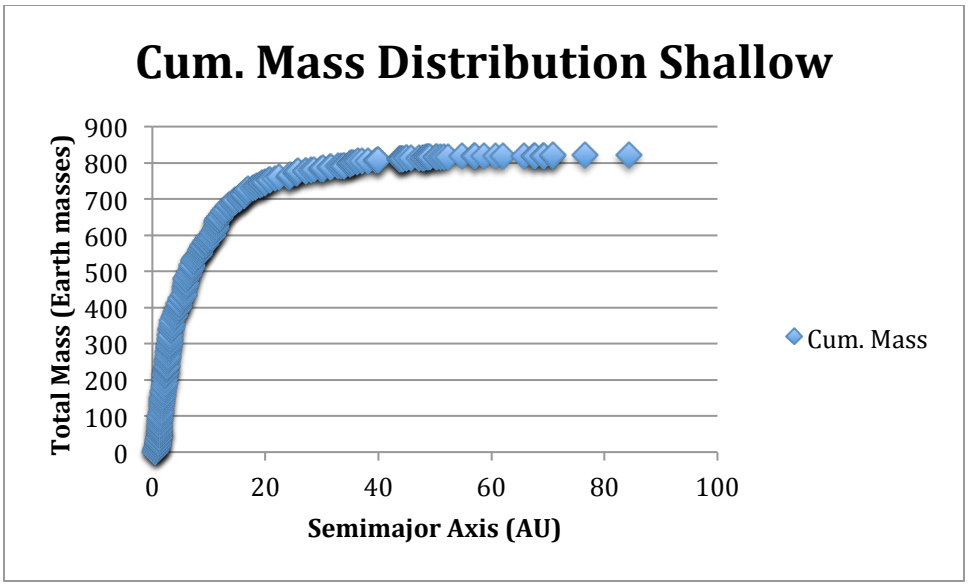

and the histogram of planet masses is:

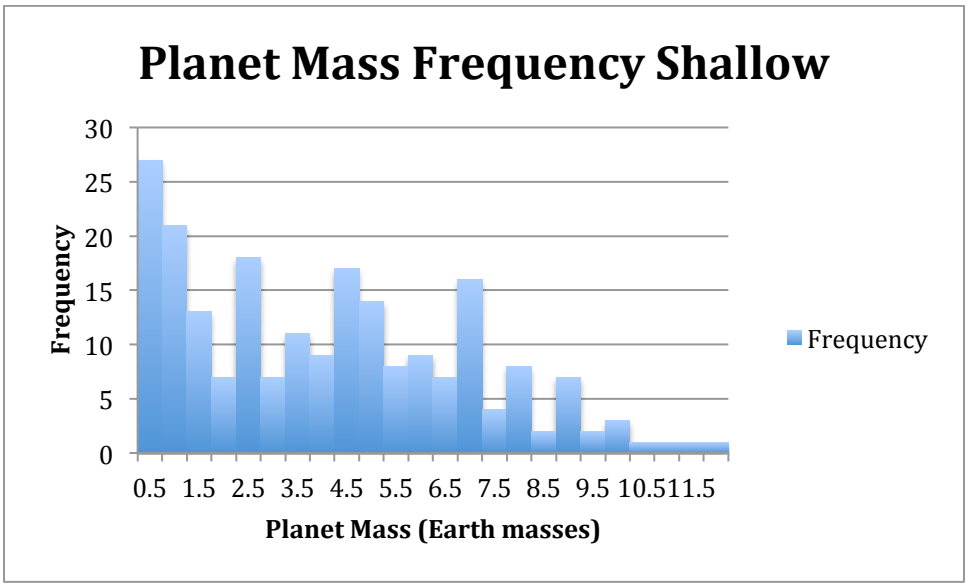

These simulations have the same disk mass as the normal case, but have a slightly shallower surface mass density profile (Σ proportional to $r^{-5/4}$). The distribution of both planet masses relative to semimajor axis and the frequency of planet masses appear to be less smooth than in the normal case. There is a similar frequency of potential Jupiters, with all 50 simulations containing a Jupiter and 20 containing multiple. The number of planets is also similar, implying that development of the disk is similar as well. The shallower distribution seems to have slightly higher planet masses and perhaps slightly shallower curves for mass frequency and mass distribution, but otherwise yields similar results to the normal case.

Finally, I will present the results for the shallower case:

Shallower	
Mean Mass	3.67
Median Mass	3.12
Mass Standard Deviation	2.768785005
Minimum Mass	0.03
Total Disk Mass	31.8378
Average Remaining Mass	16.06380369
Planet Number	219
Mean Eccentricity	0.175609998
Eccentricity Standard Deviation	0.101246967
Number of Jupiters	59
Systems with Jupiters	45
Systems with Multiple Jupiters	13

The accompanying mass distribution graphs:

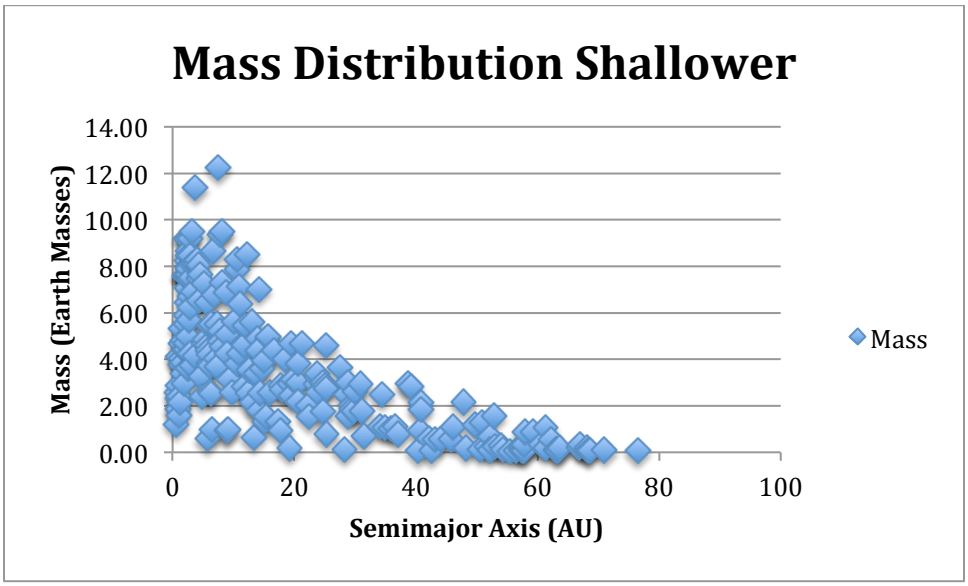

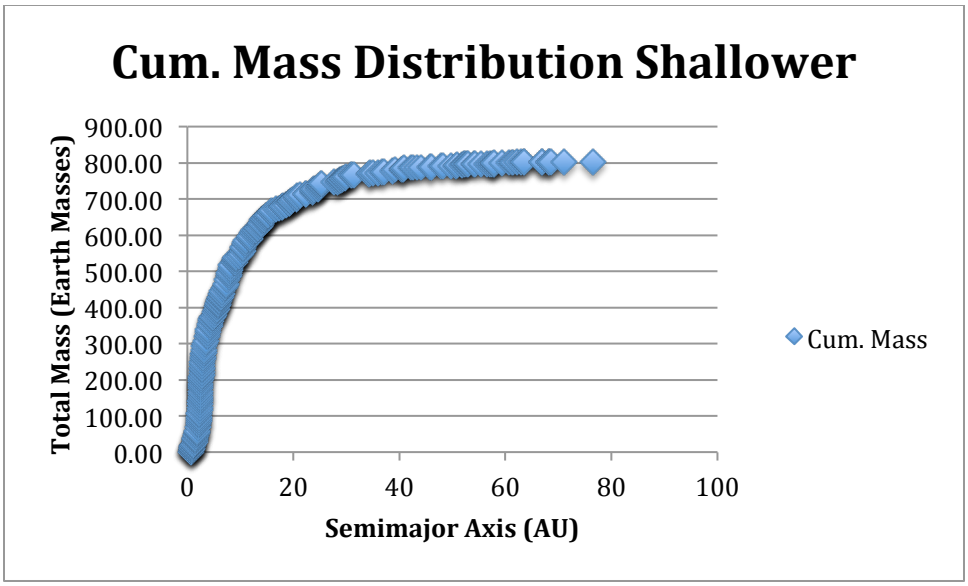

and the histogram of planet mass frequencies:

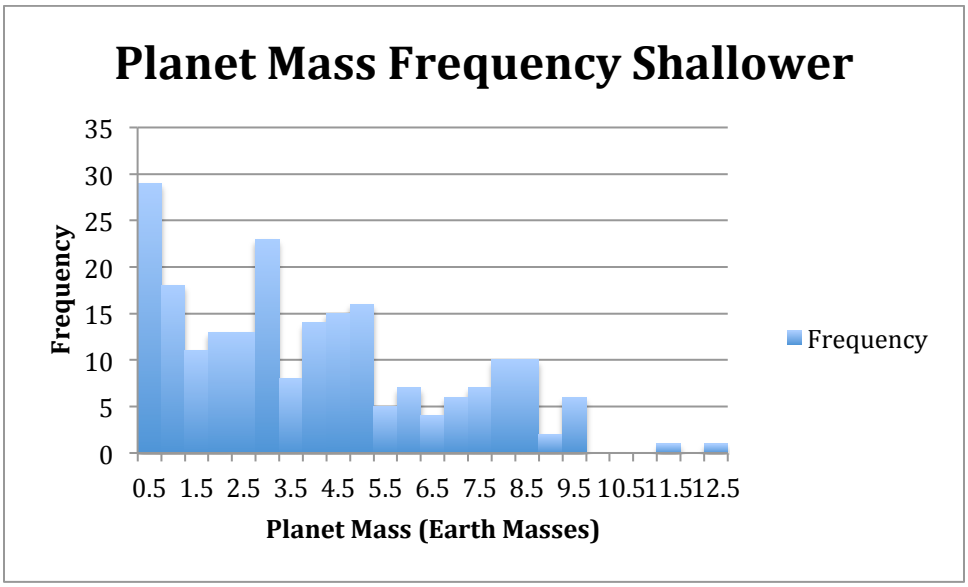

These simulations were a continuation of testing the effects of using a shallower surface mass density profile, and they had Σ proportional to r^{-1}. The distributions of both mass relative to semimajor axis and mass frequency appear to be shallower and less smooth than either the normal or shallow cases. The planet masses are closer to the planet masses in the normal case, and the frequency of Jupiters is also similar, with 45 systems out of 50 containing a Jupiter and 13 containing multiple. It seems as though the masses of the potential Jupiters do not go as high as often in this case. Additionally, the number of planets is very similar to both the normal and shallow cases as well.

Interestingly, it seems that varying the surface mass density profile doesn't result in many changes to the results. The number of planets formed is remarkably

similar (213 to 214 to 219) and the planet masses are fairly constant as well (within one third of an earth mass for the mean and median planet masses). This finding is actually at odds with the results of Raymond et al. (2009), who found that fewer planets were formed in the case where the surface mass density profile was proportion to r^{-1} when compared to $r^{-3/2}$. It seems that the shapes of the distributions are relatively maintained throughout the simulations, as shallower surface mass density profiles resulted in shallower planet distributions as well. Beyond this, however, it seems that there are no significant changes resulting from using a shallower surface mass density profile.

Conclusion:

I ran five sets of fifty simulations with the goal of characterizing likely planetary systems around M-type dwarf stars. These sets of simulations tested a range of protoplanetary disk masses and a range of surface mass density profiles to try to understand how varying these parameters would alter the resulting planetary systems. This was important to establish the characteristics of the planetary systems across a broader range of parameters. The simulations were also concerned with testing the hypothesis that M-dwarfs struggle to form gas giant planets.

The results of the simulations gave a fairly clear idea of the number and type of planets that would be formed, as well as whether or not it was possible to form gas giants. Planets massive enough to form the cores of gas giant planets were made in the vast majority of cases with a normal disk mass. Providing the gas in the disk is sufficient to create the gas giants, the simulations showed that it was probable for gas giants to form around M-type dwarf stars. They also showed higher massed terrestrial planets than are found in our solar system, consistent with other work and the results of Kepler. Just over four planets were formed on average in each planetary system. These simulations are not reliable for finding low mass planets (such as Mercury), and the time scales and eccentricities are not realistic, but the other results are still valid.

Varying the disk masses in the simulations yielded both expected and interesting results. The masses of planets formed scaled with the mass of the disk, as did the frequency of planets with sufficient masses to begin runaway gas accretion and become giant planets. No Jupiter-like planets were formed from the light disk. The disks interacted with themselves more as mass increased, likely due runaway accretion and the larger planetesimals dominating larger areas of the disk. This meant that there were fewer planets in the heavier disks. The proportion of mass remaining in planets from the protoplanetary disk scaled inversely with the mass of the disk. The resulting mass distributions seemed to grow steeper with higher massed disks.

Varying the steepness of the surface mass density profiles of the disk caused few changes beyond the steepness of the mass distribution in the resultant planetary systems. The number of planets created was nearly identical for each of the different surface mass density profiles. There were small variations in the frequency of potential giant planets between the different suites of simulations, but there were no trends and the differences were too small to for any potential trends

to be considered significant. The proportion of mass remaining in planets from the protoplanetary disk was similar between each of the different surface mass density profiles. The general trends from the surface mass density profiles were maintained relatively in the planet mass distributions. Steeper surface mass density profiles yielded steeper mass distributions, and shallower surface mass density profiles yielded shallower mass distributions. The masses of the planets remained fairly constant between the simulations as well.

The work done here lends itself to both observational and computational future work. The primary motivation behind performing these simulations was to provide an idea of what we will find as we examine these low mass stars with better telescopes, such as the James Webb Space Telescope. In this regard, these simulations should be coupled with observations of M-type dwarf stars. In addition to providing a basis for future observations, these simulations lend themselves to future computational work. Further testing masses of the disk close to the normal set of simulations would provide a better idea of what types of disk masses lead to different frequencies of Jupiter cores. Additionally, performing simulations with a varying planet mass would be useful for testing the additional parameter of planet mass. As computation power continues to improve, more simulations such as those by Ogihara and Ida (2009) and Tanaka and Ward (2004) could also be done in greater volume to obtain reasonable sample sizes while including gas in the disk. More work could be done to establish whether or not the Jupiter cores found in these simulations would actually accrete enough gas to become gas giants as well.

In conclusion, these simulations give us reason to be optimistic about the likelihood of finding planets around M-type dwarf stars. They also give us some idea of the range of values for disk masses where gas giants could occur. These simulations imply that it should be reasonably likely that we will find Jupiter-like planets around a non-negligible number of M-dwarfs. This work gives us a general idea of what to expect, while also presenting clear opportunities for future development.

Acknowledgements:

I would like to thank Ian Dell'Antonio for his help throughout this thesis, as well as for the opportunity to be a part of his lab in my time at Brown. I would also like to thank Amy Barr-Mlinar for her help in getting me started with this project and all of her suggestions throughout its early phases. The work for this thesis was funded in part by a Brown Undergraduate Teaching and Research Award.

References:

Agnor C. B. and Canup R. M. and Levison H. F. (1999) On the Character and Consequence of Large Impacts in the Late Stage of Terrestrial Planet Formation. *Icarus 142*, 219-237.

Aigrain S., Barge P., Deluil M., Fressin F., Moutou C., Queloz D., Auvergne M., Baglin A., and the CoRoT Exoplanet Science Team (2007). The CoRoT exoplanet programme: exploring the gas-giant/terrestrial planet transition. *arXiv: astro-ph/0702062v1*.

Alibert Y., Mordasini C., and Benz W. (2011) Extrasolar planet population synthesis: III. Formation of planets around stars of different masses. *Arxiv:* 1101.0513v1.

Andrews S. M. and Williams J. P. (2005) Circumstellar dust disks in Taurus-Auriga: The sub-millimeter perspective. *The Astrophysical Journal, 631,* 1134-1160.

Andrews S. M., Rosenfeld K. A., Kraus A. L., and Wilner D. J. (2013) "The Mass Dependence Between Protoplanetary Disks and their Stellar Hosts." *Arxiv:* 1305.5262v2.

Beckwith S. V. W., Sargent A. I., Chini R. S., and Guesten R. (1990) A survey for Circumstellar disks around young stellar objects. *The Astrophysical Journal, 99*, 924-945.

Borucki et al. (2010). Kepler Planet-Detection Mission: Introduction and First Results. *Science, 327* (5968): 977-980.

Boss, A. P. (1997). "Giant Planet Formation by Gravitational Instability." *Science, 276* (5320): 1836-1839.

Boss, A. P. (2006). "Rapid Formation of Super-Earths around M Dwarf Stars." *The Astrophysical Journal,* 644:L79-L82.

Chambers J. E. And Wetherill G. W. (1998) Making the Terrestrial Planets: N-Body Integrations of Planetary Embryos in Three Dimensions. *Icarus, 136*, 304-327.

Chambers J. E. (2010). "Terrestrial Planet Formation." *Exoplanets*, Sara Seager. The university of Arizona Press, 2010, Tucson, AZ.

Chambers J. E. (2013) Late Stage planetary accretion including hit-and-run collisions and fragmentation. *Icarus, 224*, 43-56.

De Pater I. and Lissauer J. J. (2010). "12.2 Detecting Extrasolar Planets." *Planetary Sciences, 2nd Edition*, de Pater and Lissauer, Cambridge University press, 2010, Cambridge, UK.

Delfosse X., Forveille T., Mayor M., Perrier C., Naef D., and Queloz D. (1998) The closest extrasolar planet: A giant planet around the M4 dwarf GL 876. *Astronomy and Astrophysics, 338*, L67-L70.

Endl M. and Cochran W. D., Kurster M, Paulson D. B., and Wittenmyer R. A., MacQueen P. J., and Tull R. G. (2006) Exploring the Frequency of Close-In Jovian Planets around M Dwarfs. *The Astrophysical Journal, 649*, 436-443.

Gaudi, B. S. (2010). "Microlensing by Exoplanets." *Exoplanets*, Sara Seager. The university of Arizona Press, 2010, Tucson, AZ.

Gould A. and Loeb A. (1992). Discovering Planetary Systems through Gravitational Microlenses. *The Astrophysical Journal*, 396: 104-114.

Hayashi C. (1981). Structure of the solar nebula, growth and decay of magnetic fields and effects of magnetic and turbulent viscosities on the nebula. *Progress of Theoretical Physics Supplements, 70*, 35-53.

Han E., Wang S. X., Wright J. T., Feng K., Zhao M., Brown J. I., and Hancock C. (2014) The Exoplanet orbit Database II: Updates to exoplanets.org. *arXiv: 1409.7709v1.*

[3]"HEC: Periodic Table of Exoplanets." Planetary Habitability Laboratory at UPR Arecibo. Published September 1, 2014. Retrieved March 10, 2015.

Hubbard W. B., Burrows A., and Lunine J. I. (2002). Theory of giant planets. *Annual Review of Astronomy and Astrophysics*, 40, 103-136.

Hubickyj O., Bodenheimer P., and Lissauer J. J. (2005). "Accretion of the gaseous envelope of Jupiter around a 5-10 Earth-mass core." *Icarus 179*, pages 415-431.

[2]"James Webb Space Telescope FAQ." NASA. n.d Retrieved March 10, 2015 from http://jwst.nasa.gov/faq.html.

Johnson J. A. and Apps K. (2009) On the Metal Richness of M Dwarfs with Planets. *The Astrophysical Journal, 699*, 933-937.

Johnson J. A. (2014) JWST Exoplanet Characterization: Big Opportunities for Small Planets around Small Stars. American Astronomical Society, AAS Meeting #223, #314.05.

[4]"Juno." JPL. NASA: Jet Propulsion Laboratory, n.d. Web. 05 Apr. 2015. http://www.jpl.nasa.gov/missions/juno/.

Kaltenegger L. And Traub W. A. (2009) Transits of Earth-Like Planets. *The Astrophysical Journal, 698*, 519-527.

Kennedy G. M. and Kenyon S. J. (2008) Planet Formation around Stars of Various Masses: The Snow Line and the Frequency of Giant Planets. *The Astrophysical Journal, 673*, 502-512.

Kenyon S. J. and Bromley B. C. (2013) Coagulations of Icy Planet Formation Around .1-.5 Solar Mass Stars: Super-Earths From Large Planetesimals. *Arxiv:* 1311.0296v1.

[1]"Kepler: About the Mission." NASA, n.d. Retrieved March 10, 2015 from http://kepler.nasa.gov/Mission/QuickGuide/.

Kokubo E. Kominami J., and Ida S. (2006) Formation of Terrestrial Planets from Protoplanets: I. Statistics of Basic Dynamical Properties. *The Astrophysical Journal, 642*, 1131-1139.

Kokubo E. And Genda H. (2010) Formation of Terrestrial Planets from Protoplanets Under a Realistic Accretion Condition. *The Astrophysical Journal Letters, 714*, L21-L25.

Laughlin G., Bodenheimer P., and Adams F. C. (2004) The Core Accretion Model Predicts Few Jovian-Mass Planets Orbiting Red Dwarfs. *The Astrophysical Journal, 612*, L73-L76.

Levine M., Shaklan S., and Kasting J. (2006). *Terrestrial Planet Finder Coronagraph: Science and Technology Definition Team (STDT) Report*. NASA/JPL Document D-34923, Jet Propulsion Laboratory, Pasadena, California.

Lissauer J. J., Dawson R. I., and Tremaine S. (2014). Advances in exoplanet science from Kepler. *Nature, 513*: 336-344.

Lovis C. and Fischer D. A. (2010). "Radial Velocity Techniques for Exoplanets." *Exoplanets*, Sara Seager. The university of Arizona Press, 2010, Tucson, AZ.

Morbidelli A., Lunine J. I., O'Brien D. P., Raymond S. N., and Walsh K. J. (2012). "Building Terrestrial Planets." *Annual Reviews of Earth and Planetary Sciences*, vol. 40, issue 1, pages 251-275.

Ogihara M. And Ida S. (2009) N-Body Simulations of Planetary Accretion around M Dwarf Stars. *The Astrophysical Journal, 699*, 824-838.

Quirrenbach, A. (2010). "Astrometric Detection and Characterization of Exoplanets." *Exoplanets*, Sara Seager. The university of Arizona Press, 2010, Tucson, AZ.

Raymond S. N., Quinn T., and Lunine J. I. (2004) Making other earths: dynamical simulations of terrestrial planet formation and water delivery. *Icarus, 168*, 1-17.

Raymond S. N., Quinn T., and Lunine J. I. (2005) The formation and habitability of terrestrial planets in the presence of close-in giant planets. *Icarus, 177*, 256-263.

Raymond S. N., Quinn T., and Lunine J. I. (2006) High-resolution simulations of the final assembly of Earth-like planets: I. Terrestrial accretion and dynamics. *Icarus, 183*, 265-282.

Raymond S. N., Scalo, J., and Meadows V. S. (2007) A Decreased Probability of Habitable Planet Formation Around Low-Mass Stars. *The Astrophysical Journal, 669*, 606-614.

Raymond S. N., O'Brien D. P., Morbidelli A., and Kaib N. A. (2009) Building the terrestrial planets: Constrained accretion in the inner Solar System. *Icarus, 203*, 644-662.

Raymond S. N., Kokubo E., Morbidelli A., Morishima R., and Walsh K. J. (2014) Terrestrial Planet Formation at Home and Abroad. *Arxiv:* 1312.1689v3.

Redy, F. (2014, May 19). Q&A Session about NASA's WFIRST Mission. Retrieved March 10, 2015 from http://www.nasa.gov/content/goddard/qa-session-about-nasas-wfirst-mission/#.VQeVRhDF-vJ.

Ricker et al. (c. 2014) The Transiting Exoplanet Survey Satellite Mission. American Astronomical Society, AAS Meeting #224, #113.02

Rivera E. J., Lissauer J. J., Butler, R. P., Marcy G. W., Vogt S. S., Fischer D. A., Brown T. M., Laughlin G., and Henry G. W. (2005) A ~7.5 Earth-Mass Planet Orbiting the Nearby Star GJ 876. *ArXiv: astro-ph/0510508v2.*

Roberge and Kamp (2010). "Protoplanetary and Debris Disks." *Exoplanets*, Sara Seager. The university of Arizona Press, 2010, Tucson, AZ.

Seager S. and Lissauer J. J. (2010). "Introduction to Exoplanets." *Exoplanets*, Sara Seager. The university of Arizona Press, 2010, Tucson, AZ.

Segura A. and Kalteneggar L. (2009). "Chapter 14: Search for Habitable Planets." *Astrobiology: Emergence, Search and Detection of Life*, V.A. Basiuk. American Scientific Publishers.

Spergel D., Gehrels N., et al. (2013). WFIRST-AFTA Final Report by the Science Definition Team (SDT) and WFIRST Project. *arXiv: 1305.5422*.

Swain M. R. (2012). The FINESSE Mission. American Astronomical Society, AAS Meeting #200, #505.05.

Tanaka H. and Ward W. R. (2004) Three-Dimensional Interaction Between a Planet and an Isothermal Gaseous Disk: II. Eccentricity Waves and Bending Waves. *The Astrophysical Journal, 602*, 388-395.

Traub W. A. and Oppenheimer B. R. (2010). "Direct Imaging of Exoplanets." *Exoplanets*, Sara Seager. The university of Arizona Press, 2010, Tucson, AZ.

Winn J. N. (2010). "Exoplanet Transits and Occultations." *Exoplanets*, Sara Seager. The university of Arizona Press, 2010, Tucson, AZ.

Wolszczan A. and Kuchner M. J. (2010). "Planets Around Pulsars and Other Evolved Stars: The Fates of Planetary Systems." *Exoplanets*, Sara Seager. The university of Arizona Press, 2010, Tucson, AZ.

Appendix 1:

```
#Python Script to generate a protoplanetary disk
#Distance in AU, time in days, and mass such that
#1 solar mass = 2.95913976899595E-04

#Generates a proto planetary disk of equal massed planetesimals.
#The planetesimals follow a r^-.5 distribution, as expected for a disk
#following a r^-1.5 surface mass density distribution.
def main():
	#Import necessary modules
	import random
	import math
	#Star parameters
	Solar_Mass = 2.95913976899595E-04
	star_mass = Solar_Mass/3
	#Disk parameters
	r_min = .05
	r_max = 30
	gas_to_solid = 70
	disk_to_star = .02
	disk_mass = star_mass*disk_to_star/gas_to_solid
	#Planetesimal parameters
	planetesimal_number = 10**3
	planetesimal_density = 3 #g/cm^3
	#Computation pre-processing
	r_range = r_max-r_min
	planetesimal_mass = disk_mass/planetesimal_number
	density_conversion = 498.24107635393868
	planetesimal_radius =
(3*planetesimal_mass/(4*math.pi*planetesimal_density*density_conversion))**(1.0
/3.0)
	hill_radius_constant = (planetesimal_mass/(3*star_mass))**(1.0/3.0)
	positions = []
	#File set-up
	pl = open("pl.in", "w")
	pl.write(str(1+planetesimal_number)+"\n")
	pl.write("1 "+(str(star_mass)).upper()+"\n")
	pl.write(".0 .0 .0\n.0 .0 .0\n")
	#Iteration to create disk file
	i = 0
	while i < planetesimal_number:
		#Radius calculation
		rand = (random.random()**2.0)
		radius = r_min+r_range*rand
		#Hill Radius Computation
```

```
                hill_radius = radius*hill_radius_constant
                #Cartesian Representation Computation
                angle = random.random()*2*math.pi
                x = math.cos(angle)*radius
                y = math.sin(angle)*radius
                #Cartesian Velocity Computation
                orbital_velocity = (star_mass/radius)**(1/2.0)
                vx = math.cos(angle+math.pi/2)*orbital_velocity
                vy = math.sin(angle+math.pi/2)*orbital_velocity
                if is_valid(x, y, hill_radius**2, positions):
                        #Write to file
                        pl.write(str(2+i)+" "+str(planetesimal_mass).upper()+"
"+(str(hill_radius)).upper()+"\n")
                        pl.write(str(planetesimal_radius).upper()+"\n")
                        pl.write((str(x)).upper()+" "+(str(y)).upper()+" 0.0\n")
                        pl.write(str(vx).upper()+" "+str(vy).upper()+" 0.0\n")
                        #Add position and move forward in loop
                        temp_pos = [x,y,hill_radius**2]
                        positions.append(temp_pos)
                        i += 1
                else:
                        print("Rejected!")
        #Finished disk creation
        pl.close()
        print("disk created")

#returns true if a position is valid
#returns false if a position is within another object's hill sphere
def is_valid(x, y, r, arr):
        for pos in arr:
                distance = (x-pos[0])**2+(y-pos[1])**2
                if distance < pos[2]:
                        return False
                if distance < r:
                        return False
        return True
main()
```

Appendix 2:

The following table presents the results of the individual simulations with a surface mass density proportional to $r^{-3/2}$ and a disk-to-mass ratio of .02.

Normal				
Simulation Number	Number of Planets	Mass	Semimajor Axis (AU)	Eccentricity
1	3	2.83	8.1768	0.2849
		9.73	2.9253	0.5115
		0.954	50.1286	0.3448
2	7	0.254	37.6209	0.0344
		5.15	0.9719	0.2172
		0.731	28.7796	0.1024
		0.0317	76.4356	0.1518
		4.64	4.9939	0.1371
		0.0317	62.663	0.1616
		3.47	13.5365	0.0252
3	5	2.54	0.8321	0.3313
		0.542	59.4329	0.2507
		4.11	14.049	0.1137
		3.78	5.2947	0.1562
		5.12	2.1913	0.072
4	4	5.34	1.891	0.2658
		0.0317	8.3263	0.4289
		0.477	42.1791	0.1763
		3.38	18.7293	0.2214
5	5	2.83	0.8629	0.3345
		2.57	15.5038	0.022
		5.98	2.1533	0.2302
		0.318	32.9794	0.3514
		3.02	5.9328	0.3531
6	3	10.34	1.4832	0.1052
		3.97	14.7202	0.1412
		3.15	7.0299	0.1155
7	4	5.95	1.5088	0.1832
		2.29	4.9501	0.0452
		0.7314	40.1143	0.1051
		4.74	18.0312	0.0478
8	4	0.954	49.6446	0.3382
		6.68	2.8529	0.234
		7.03	12.4258	0.0761
		3.53	1.1716	0.1886

9	4	3.33	16.823	0.0881
		7.22	1.8321	0.2154
		0.763	53.2762	0.3194
		5.5	7.1389	0.0508
10	3	6.68	1.6761	0.3944
		0.508	39.8544	0.3672
		3.75	13.1553	0.0528
11	3	11.3	2.9889	0.1295
		2.52	20.7242	0.1327
		3.18	8.9365	0.1327
12	4	8.97	5.944	0.0896
		1.31	29.563	0.1252
		0.254	58.4729	0.2796
		5.44	1.5242	0.5626
13	4	0.0635	53.6166	0.1403
		6.58	8.1402	0.1317
		0.858	17.7316	0.3682
		5.25	1.1747	0.3168
14	3	6.61	1.0175	0.1682
		0.35	54.7035	0.4494
		8.36	6.0385	0.0661
15	6	0.159	36.6028	0.2379
		3.38	6.6637	0.2307
		5.37	3.3011	0.2211
		1.56	0.7292	0.1986
		0.0317	65.972	0.2182
		2.92	19.4037	0.1014
16	4	3.03	23.4283	0.1503
		0.318	12.0122	0.2263
		3.12	3.3943	0.1132
		4.29	6.8988	0.067
17	4	3.15	14.6923	0.1153
		5.88	5.6756	0.0966
		1.02	21.3731	0.0699
		7.19	1.9378	0.1542
18	4	3.12	8.2725	0.3058
		1.37	20.1014	0.0399
		0.731	59.1038	0.4804
		9.01	2.1863	0.1592
19	4	1.43	14.1319	0.3009
		4.13	7.317	0.0747
		2.51	29.0234	0.1446

		10.2	1.0646	0.2181
20	5	1.17	29.0153	0.1893
		3.78	3.8793	0.2184
		5.69	7.6498	0.2095
		0.637	46.1106	0.3109
		4.48	0.9711	0.2851
21	4	0.86	42.7343	0.4412
		6.93	1.7522	0.275
		2.54	4.8495	0.0935
		4.74	14.3113	0.1429
22	4	10.24	3.1398	0.1762
		0.67	6.3153	0.1667
		2.33	23.647	0.2074
		0.58	50.9329	0.2851
23	2	9.99	4.5726	0.3636
		0.51	42.4074	0.6448
24	4	7.82	2.1162	0.0689
		0.48	33.4018	0.3281
		2.26	19.4635	0.1253
		5.21	7.927	0.1113
25	5	5.57	9.3066	0.1013
		0.41	52.4264	0.154
		2.77	15.5674	0.1905
		1.68	0.7467	0.3522
		5.22	2.28	0.1391
26	4	0.51	5.6096	0.0967
		5.88	10.4913	0.046
		8.05	2.8322	0.2074
		1.02	33.3417	0.2245
27	5	4.55	5.7068	0.0464
		0.25	65.617	0.2824
		5.11	1.9802	0.1416
		1.90	31.6952	0.1134
		3.17	11.5646	0.0691
28	4	0.32	37.5278	0.2051
		3.41	5.0669	0.0908
		0.06	58.9629	0.0266
		5.83	12.7831	0.0459
29	3	2.36	29.1835	0.3115
		4.52	0.655	0.38
		9.87	4.2204	0.0147
30	4	0.06	54.9705	0.4483

		2.38	23.5876	0.1473
		4.29	7.6764	0.1739
		10.43	3.0103	0.2238
31	3	2.48	4.5167	0.1109
		3.66	8.848	0.2592
		0.795	23.6246	0.1436
32	5	6.37	3.6843	0.2709
		6.37	0.9746	0.1256
		4.97	11.6372	0.0881
		0.666	35.4181	0.0903
		0.0317	67.0998	0.0797
33	4	2.29	30.7633	0.1547
		7.92	1.5065	0.1361
		6.87	8.2781	0.1095
		0.0954	53.8337	0.1022
34	4	6.52	6.3582	0.1912
		3.59	2.3068	0.2006
		1.524	31.8132	0.035
		0.0637	55.9258	0.1132
35	4	4.32	10.8807	0.1343
		4.1	4.1775	0.1218
		8.43	1.3439	0.0522
		0.637	48.5956	0.5295
36	4	6.04015	2.515	0.5345
		2.258	24.1	0.2616
		0.381602	53.3255	0.1944
		3.62409	6.5664	0.2439
37	6	0.827557	33.1798	0.179
		1.17416	6.4216	0.061
		7.03367	2.4451	0.1447
		3.2741	10.7702	0.05
		2.67573	18.6901	0.0821
		0.0318378	65.2364	0.0903
38	4	2.89024	24.735	0.1356
		10.7255	2.6315	0.1985
		0.127577	60.154	0.4505
		1.30964	5.0104	0.3255
39	5	2.32574	15.591	0.0864
		2.73218	8.8447	0.1473
		0.636756	55.0544	0.3131
		7.09012	3.9775	0.1269
		4.00795	0.6068	0.2931

40	6	3.14991	2.2454	0.04
		4.77567	4.8279	0.0766
		3.88376	1.1106	0.0948
		2.51767	8.6499	0.0909
		2.99185	17.9096	0.0725
		0.190801	56.9156	0.236
41	3	5.79	4.2459	0.313
		3.94	23.0857	0.2626
		5.67	1.4724	0.1519
42	3	2.38	35.935	0.1446
		7.44	1.2655	0.327
		2.42	7.1357	0.245
43	5	0.0954	49.2738	0.426
		3.31	19.45	0.1108
		3.94	5.1348	0.1846
		7.86	1.0974	0.0809
		2.61	9.2917	0.2086
44	5	0.318	30.6782	0.0764
		1.31	46.3046	0.1705
		2.68	15.9323	0.1145
		6.11	0.7384	0.2017
		6.65	3.8829	0.0477
45	6	0.509	51.8627	0.145
		2.19	10.9383	0.077
		0.922	22.6855	0.0577
		4.52	1.0917	0.1375
		1.31	8.4498	0.0655
		7.89	4.0118	0.0965
46	5	0.99	11.259	0.1136
		0.45	72.1026	0.1115
		1.49	36.2383	0.177
		3.97	6.6977	0.1096
		6.33	2.3846	0.2196
47	6	3.97	5.5662	0.2224
		0.76	41.3505	0.1749
		7.47	1.2615	0.4126
		1.05	22.423	0.0933
		4.67	14.732	0.0244
		0.03	73.3765	0.1703
48	3	8.21	6.9445	0.1411
		0.25	40.6867	0.2663
		7.63	1.5522	0.1529

49	6	3.92	8.0795	0.0713
		3.12	0.6204	0.263
		6.02	2.5881	0.1779
		0.19	15.4587	0.1412
		0.03	58.5394	0.142
		3.03	31.2234	0.117
50	4	10.50	1.945	0.1272
		2.22	30.8521	0.1832
		1.37	4.7983	0.1553
		5.02	10.8168	0.0221

Appendix 3:

The following table presents the results of the individual simulations with a surface mass density proportional to $r^{-3/2}$ and a disk-to-mass ratio of .005.

Light				
#	Planet #	Mass	Radius	Eccentricity
1	5	1.62576	4.6347	0.1881
		0.613047	2.426	0.3551
		0.34999	16.2304	0.413
		0.572403	37.5923	0.243
		1.081582	0.9276	0.3797
2	5	0.302572	23.3967	0.4459
		1.47899	14.3337	0.1707
		1.76124	1.8452	0.1273
		2.19026	4.0994	0.144
		0.246122	47.6741	0.1287
3	5	1.30964	7.7187	0.0166
		0.0159189	80.92	0.1452
		1.081582	25.2845	0.5461
		1.6935	3.2451	0.2541
		0.930296	1.6548	0.1051
4	7	0.00795945	55.727	0.38
		1.52415	9.5936	0.1759
		0.851266	9.5936	0.1759
		0.27096	30.7274	0.0879
		0.6774	17.4608	0.0702
		0.00795945	55.1003	0.2953
		1.82898	1.0762	0.1668
5	4	0.906587	5.9408	0.4044
		0.318378	29.2264	0.0819
		1.74995	2.2164	0.0819
		1.14029	12.8261	0.1251
6	4	1.50157	12.6293	0.1815
		2.00962	1.4429	0.3017
		1.44512	4.9356	0.193
		0.668368	25.862	0.2977
7	4	2.0322	4.6963	0.0772
		1.54673	0.668	0.4237
		0.946102	12.0801	0.0287
		0.21451	38.8126	0.3579
8	5	0.0318378	16.6786	0.2051
		1.95317	2.8041	0.1916

		0.0159189	49.0255	0.1097
		1.089485	11.9168	0.2144
		0.803848	31.3035	0.1963
9	6	0.294669	54.4416	0.3419
		1.097388	10.058	0.1507
		0.469664	2.4534	0.1356
		1.30964	1.3576	0.2668
		1.50157	5.9354	0.1381
		0.572403	23.279	0.2958
10	4	0.946102	3.0255	0.4127
		1.5806	5.9097	0.0534
		0.263057	43.4379	0.1383
		1.27577	21.8478	0.0664
11	5	0.342087	36.2424	0.3904
		1.79511	4.4947	0.1343
		1.67092	15.495	0.0586
		1.96446	1.2975	0.2592
		0.286766	9.605	0.2405
12	4	1.5806	15.0846	0.0612
		2.40477	2.2861	0.049
		0.278863	28.2838	0.3665
		0.0795945	9.0847	0.2338
13	5	2.41606	4.5819	0.3287
		0.0238219	62.6839	0.164
		1.19674	1.0812	0.2639
		0.286766	35.5573	0.0734
		0.803848	12.65	0.2734
14	6	1.23061	12.4656	0.1806
		0.302572	39.2072	0.3413
		0.119674	30.1312	0.2988
		3.13862	2.9381	0.3119
		0.00795945	30.4975	0.4981
		0.00795945	8.0078	0.0848
15	4	0.0954005	37.5123	0.2566
		1.04997	18.7701	0.1842
		2.39348	2.2937	0.5152
		2.38219	7.2364	0.3301
16	6	1.14029	1.6845	0.0458
		1.17416	4.6742	0.0565
		0.0318378	8.8979	0.1338
		0.548694	0.836	0.237
		0.190801	33.6307	0.3405

		2.54025	14.3333	0.0658
17	6	0.438052	19.4143	0.2578
		0.859169	0.4228	0.2202
		1.63705	11.4849	0.0372
		0.151286	54.7325	0.3496
		0.0477567	4.6417	0.1354
		1.79511	3.2506	0.0124
18	5	1.14029	5.3385	0.106
		0.731592	11.2242	0.1586
		2.19026	1.542	0.2979
		0.42902	45.7412	0.5252
		0.637885	8.1804	0.1057
19	7	1.5806	17.9442	0.0467
		0.413214	11.3645	0.3066
		1.72737	4.983	0.0922
		0.127577	54.137	0.017
		0.938199	0.07892	0.1376
		0.827557	2.7738	0.0112
		0.21451	35.7752	0.1785
20	5	0.13548	69.0108	0.2781
		0.0954005	48.1035	0.3335
		1.62576	0.9614	0.412
		2.00962	5.2121	0.1528
		1.52415	18.2453	0.1376
21	6	1.089485	13.3485	0.0967
		0.91449	23.4896	0.0562
		1.097388	1.5983	0.14
		1.87414	5.1782	0.0834
		0.190801	37.2594	0.0449
		0.0954005	2.9029	0.1142
22	8	0.310475	30.7577	0.1135
		1.60318	15.6867	0.044
		0.48547	8.5692	0.0994
		0.0238219	57.6963	0.1385
		0.0159189	62.6962	0.0361
		0.739495	0.788	0.3393
		0.00795945	40.7689	0.3838
		2.38219	3.7983	0.3293
23	8	0.604015	23.0743	0.1153
		0.91449	10.9881	0.1471
		0.302572	30.6039	0.0661
		1.81769	1.3412	0.3331

		0.0795945	44.5575	0.2824
		0.938199	3.4904	0.2559
		0.0318378	64.7758	0.1135
		0.827557	6.4764	0.079
24	5	1.59189	1.2169	0.1119
		0.867072	9.6663	0.0874
		0.365796	35.4883	0.2151
		1.89672	5.3379	0.1026
		0.954005	15.6756	0.0875
25	7	1.15158	0.6259	0.1209
		0.0873846	41.3677	0.3789
		0.00795945	52.9639	0.2945
		1.30964	5.7148	0.14
		1.43383	12.6379	0.0769
		1.2419	2.7225	0.151
		0.692077	23.5824	0.0501
26	5	1.74995	3.1908	0.1025
		1.18545	0.6042	0.0544
		0.1034164	43.4192	0.352
		1.26448	17.891	0.1011
		1.4677	8.5867	0.0919
27	7	0.198704	49	0.0898
		1.018358	13.258	0.1011
		0.198704	31.859	0.1031
		1.65963	2.1884	0.3252
		1.52415	7.8951	0.0838
		0.00795945	55.5108	0.0365
		0.715786	0.7733	0.1731
28	4	2.1451	1.132	0.2467
		0.580306	26.0674	0.1164
		0.890781	3.5794	0.2941
		1.59189	8.7379	0.0984
29	4	2.46122	1.7282	0.1858
		0.636756	20.5628	0.2518
		0.206607	38.3267	0.0866
		2.22413	7.62	0.1292
30	8	1.70479	2.7334	0.0865
		0.684174	24.8664	0.0505
		0.0556597	4.6075	0.2594
		0.0238219	56.6113	0.3662
		1.14029	0.8823	0.2677
		1.62576	13.4785	0.0187

		0.286766	16.3525	0.1393
		0.00795945	57.4852	0.2227
31	6	1.002552	0.4568	0.1294
		1.77253	5.5667	0.1308
		0.143383	47.3573	0.1672
		0.859169	15.0294	0.233
		0.373699	29.573	0.0642
		1.49028	3.2724	0.2383
32	7	0.572403	0.7101	0.2187
		1.52415	2.5369	0.1058
		1.82898	12.0931	0.123
		0.469664	21.5982	0.1624
		0.151286	66.8136	0.3454
		0.954005	5.4553	0.2375
		0.00795945	48.9274	0.1393
33	4	1.27577	1.1619	0.2917
		2.12252	3.0811	0.1428
		0.715786	34.0191	0.2277
		2.1451	12.2982	0.0738
34	10	1.29835	6.7647	0.1167
		0.580306	0.8669	0.1855
		1.37738	3.5733	0.0663
		0.0159189	29	0.3106
		1.010455	14.5241	0.1171
		0.00795945	36.2257	0.3425
		0.00795945	69.1951	0.1737
		0.00795945	60.4529	0.4878
		0.00795945	35.9975	0.1562
		0.00795945	62.9425	0.5192
35	5	1.33222	1.9833	0.2473
		1.29835	4.2834	0.1938
		0.747398	0.4813	0.2734
		1.30964	9.894	0.1295
		0.182898	50.8074	0.1226
36	4	0.636756	31.0759	0.3211
		3.08217	2.401	0.1702
		1.52415	9.2277	0.242
		0.246122	17.064	0.1564
37	5	0.636756	25.3563	0.225
		0.890781	0.9934	0.5864
		1.23061	12.19	0.1034
		0.0238219	40.2803	0.2865

		2.46122	4.7478	0.0383
38	5	0.851266	13.4347	0.0552
		0.198704	25.1372	0.1225
		0.286766	7.5631	0.1477
		0.167092	31.1773	0.0223
		1.39996	5.7495	0.0796
39	3	1.95317	7.2975	0.0133
		1.15158	19.0505	0.0394
		2.1451	1.8798	0.1306
40	6	1.065776	8.1276	0.1531
		1.33222	20.5789	0.0826
		0.0556597	41.882	0.3241
		1.70479	2.1683	0.0375
		0.254025	42.4597	0.0791
		0.859169	0.7099	0.2664
41	6	0.978843	1.796	0.3154
		0.771107	4.3536	0.1629
		1.44512	9.4751	0.1273
		0.0715786	43.47	0.3604
		0.850137	15.15	0.1045
		1.089485	0.8913	0.1413
42	7	1.65963	4.6802	0.0984
		0.978843	8.0372	0.1211
		0.1034164	57.2918	0.4739
		0.963037	1.5543	0.0356
		0.994649	15.6398	0.0713
		0.159189	0.4782	0.0558
		0.636756	26.6065	0.0711
43	6	0.0397408	32.8771	0.1331
		0.13548	43.5262	0.0982
		0.524985	1.4792	0.0713
		0.69998	24.9167	0.0516
		1.042067	2.9143	0.2011
		2.05478	8.2959	0.168
44	5	0.0397408	67.8226	0.3496
		1.95317	11.1336	0.1061
		0.509179	33.5879	0.2071
		1.99833	3.0473	0.0525
		1.129	0.8864	0.2912
45	5	1.90801	10.1331	0.1187
		0.652562	23.493	0.1459
		0.0318378	53.4324	0.0878

		0.556597	0.7484	0.2085
		0.978843	3.1432	0.1546
46	7	0.946102	5.561	0.1185
		0.572403	0.8628	0.0211
		0.692077	1.4889	0.1257
		1.32093	3.2407	0.1183
		1.41125	17.2063	0.0242
		0.0556597	36.5898	0.2801
		0.00795945	48.8136	0.3071
47	4	0.819654	0.977	0.0433
		2.89024	3.4779	0.2529
		0.859169	16.1543	0.1811
48	3	1.081582	18.2942	0.4399
		0.00795945	56.2433	0.2547
		4.22246	3.8398	0.3489
49	6	0.48547	11.2315	0.1897
		0.795945	24.2023	0.1879
		0.0159189	44.36	0.3026
		1.034164	0.63	0.4842
		0.119674	47.5147	0.2211
		2.84508	6.0105	0.1475
50	5	1.68221	1.2253	0.1885
		1.129	4.6499	0.153
		0.413214	39.5144	0.4556
		1.002552	5.8535	0.002
		1.21932	13.0686	0.1265

Appendix 4:

The following table presents the results of the individual simulations with a surface mass density proportional to $r^{-3/2}$ and a disk-to-mass ratio of .1.

Heavy				
#	Planet #	Mass	Radius	Eccentricity
1	2	13.58	10.4759	0.2141
		25.62	2.044	0.2298
2	4	1.59	36.8805	0.1035
		11.29	6.3283	0.1461
		14.32	14.0233	0.1273
		23.07	2.5606	0.1223
3	5	7.00	6.9868	0.108
		1.59	26.7374	0.2163
		17.83	14.0732	0.1516
		0.32	64.4337	0.3685
		38.50	1.9478	0.1377
4	4	1.75	40.2322	0.2825
		23.07	1.431	0.1792
		1.43	21.5673	0.2457
		17.97	4.8867	0.1067
5	4	4.13	25.1397	0.1339
		2.07	76.2685	0.1385
		20.21	11.5208	0.2249
		37.07	2.1795	0.1737
6	3	21.79	2.1186	0.0427
		21.47	10.193	0.1124
		4.93	19.8325	0.0826
7	5	1.11	37.9179	0.1968
		17.66	8.9875	0.0996
		2.38	31.4114	0.1386
		0.16	66.0024	0.142
		0.16	87.3946	0.0578
8	3	1.75	41.3647	0.4544
		28.80	5.6911	0.104
		21.00	1.86	0.2492
9	4	8.12	15.1965	0.2549
		2.71	39.6943	0.2407
		10.50	7.699	0.1736
		20.68	1.6257	0.0604
10	4	14.79	7.0685	0.104
		25.93	2.4357	0.1288

		3.66	21.9994	0.2124
		0.48	52.9868	0.2134
11	2	11.62	33.3587	0.1607
		40.56	4.3359	0.4872
12	3	13.84	22.2949	0.1522
		23.71	4.7497	0.1208
		0.95	48.7605	0.0829
13	4	0.64	66.3765	0.0684
		11.13	7.9094	0.2755
		34.05	1.5716	0.067
		10.66	23.6266	0.4229
14	4	25.13	1.424	0.4059
		4.92	21.3794	0.4169
		9.22	8.6427	0.1977
		3.34	61.9922	0.2308
15	2	5.72	44.5976	0.3187
		37.71	1.7612	0.2067
16	4	19.57	10.9793	0.029
		15.75	0.7872	0.1013
		19.41	2.3443	0.2151
		2.87	54.6195	0.4629
17	3	30.87	1.7674	0.2817
		14.47	11.4548	0.0868
		3.50	39.5536	0.0805
18	5	6.37	16.5666	0.3535
		10.03	6.159	0.167
		2.38	51.2402	0.4478
		29.12	2.4369	0.1143
		16.71	0.798	0.1378
19	4	42.16	2.2347	0.3574
		6.84	12.9178	0.1679
		3.34	47.1329	0.1715
		3.66	21.322	0.1345
20	3	0.64	53.0829	0.2986
		42.80	1.995	0.1896
		11.13	13.7883	0.1351
21	3	0.16	44.601	0.242
		42.31	1.7263	0.3653
		14.63	11.3755	0.0913
22	4	23.54	1.5403	0.1535
		25.13	5.0214	0.2089
		12.88	14.9647	0.3004

		0.80	47.5068	0.2076
23	2	14.96	0.7302	0.2062
		35.63	8.0845	0.1823
24	3	8.12	32.3214	0.5184
		4.46	11.5334	0.0746
		46.77	2.9291	0.2233
25	5	12.57	12.0542	0.1038
		21.32	3.649	0.0764
		23.38	1.1334	0.2123
		0.80	55.3695	0.1282
		4.62	29.0178	0.1124
26	4	21.47	6.7246	0.108
		31.18	0.13445	0.1963
		3.50	51.8704	0.3122
		6.68	18.9877	0.3189
27	5	7.96	32.164	0.0486
		20.53	4.6756	0.0993
		17.82	0.15618	0.2291
		0.16	59.0264	0.088
		8.75	12.7086	0.2503
28	2	6.84	16.3303	0.46
		56.80	3.3491	0.6222
29	3	19.88	6.3985	0.1107
		8.43	16.7753	0.0303
		19.41	2.305	0.1946
30	4	18.62	7.4001	0.2125
		35.80	2.3303	0.2415
		4.29	33.5176	0.0993
		0.16	45.9807	0.1985
31	3	15.43	6.7631	0.0829
		35.63	1.3196	0.4317
		11.13	36.1013	0.2194
32	4	3.66	38.3364	0.3904
		8.59	8.9007	0.1349
		6.37	18.4849	0.3633
		32.46	2.982	0.0838
33	3	23.38	1.5326	0.1204
		18.13	5.3126	0.1918
		1.28	49.3522	0.0911
34	2	38.02	2.4563	0.5127
		23.38	20.1381	0.0189
35	5	2.22	21.2179	0.2601

		26.41	1.0503	0.3363
		5.72	10.1405	0.056
		21.96	5.5239	0.1251
		1.91	53.2117	0.3818
36	4	28.63	1.1389	0.2704
		1.74	37.8701	0.2316
		14.47	3.6716	0.1643
		12.09	13.6481	0.2422
37	2	17.03	9.5304	0.067
		35.80	2.3364	0.0757
38	3	2.87	31.4743	0.3249
		38.82	1.9423	0.2366
		14.96	13.9098	0.1601
39	3	1.43	53.303	0.3469
		49.16	8.1988	0.742
		2.87	26.6448	0.3535
40	3	0.16	60.1556	0.1766
		44.06	2.4469	0.1229
		6.84	29.2673	0.238
41	4	9.87	10.8743	0.0731
		0.80	41.5521	0.0505
		27.21	3.7595	0.0421
		17.82	0.971	0.1088
42	3	7.47	38.4959	0.6355
		7.16	4.8766	0.4001
		5.72	1.4675	0.1059
43	4	5.88	16.3984	0.2621
		23.87	6.7851	0.0544
		30.38	0.9483	0.1688
		3.66	47.8898	0.1591
44	4	0.16	69.2863	0.0766
		28.32	1.5909	0.2776
		9.22	16.9641	0.108
		16.22	5.2796	0.337
45	4	10.97	18.679	0.0657
		21.16	4.7076	0.2233
		1.11	46.2348	0.4976
		25.29	1.238	0.2771
46	2	14.00	26.1982	0.2899
		33.41	3.2199	0.0882
47	3	0.64	42.9448	0.2694
		19.72	3.911	0.0794

		14.32	15.6767	0.1677
48	3	7.32	21.4878	0.146
		4.93	10.9852	0.3249
		36.12	3.684	0.1153
49	4	44.22	1.7968	0.0676
		17.03	7.1843	0.1175
		4.78	29.3982	0.166
		0.95	51.0314	0.1514
50	5	34.52	1.5887	0.0787
		0.80	39.6913	0.1542
		36.27	7.7517	0.0941
		1.91	27.131	0.0742
		3.18	15.0456	0.1952

Appendix 5:

The following table presents the results of the individual simulations with a surface mass density proportional to $r^{-5/4}$ and a disk-to-mass ratio of .02.

Shallow				
#	Planet #	Mass	Radius	Eccentricity
1	4	4.7418	21.6879	0.1069
		8.94168	2.233	0.2096
		0.0318378	67.4636	0.3523
		4.00795	7.8485	0.0327
2	3	4.00795	12.067	0.2782
		9.86746	3.8182	0.513
		0.540791	48.084	0.1518
3	6	3.81602	16.2529	0.1925
		1.2419	28.6883	0.1065
		0.127577	65.7731	0.3215
		1.20803	10.43	0.1654
		2.22413	1.0177	0.0264
		7.76752	3.0717	0.1997
4	3	7.03367	4.3183	0.2512
		1.30964	43.7848	0.2137
		2.64186	12.7358	0.2577
5	4	2.06607	16.2223	0.394
		2.06607	36.235	0.1392
		4.54987	4.4479	0.1411
		5.56597	1.7256	0.199
6	3	5.7579	9.8258	0.154
		2.22413	22.4585	0.1029
		7.89171	2.0501	0.0201
7	4	1.33222	39.9302	0.5256
		0.763204	44.1855	0.2494
		4.67406	2.9765	0.0895
		6.64981	5.976	0.0576
8	5	3.56764	1.3147	0.1871
		8.2417	6.046	0.0176
		2.38219	2.5862	0.2641
		0.127577	48.7246	0.3352
		1.68221	28.0873	0.1029
9	6	2.22413	0.7911	0.1315
		4.04182	2.3911	0.0706
		0.381602	69.3197	0.2411
		7.63204	4.9944	0.0777

		0.318378	37.0598	0.2246
		5.15953	11.3206	0.0712
10	5	0.0954005	49.0683	0.2808
		3.59022	18.4938	0.0568
		3.05959	4.6199	0.15
		6.96593	2.0282	0.1798
		2.22413	9.5438	0.1924
11	5	4.2902	2.4685	0.2133
		1.68221	35.1029	0.2597
		5.66758	11.3913	0.1753
		3.59022	1.2497	0.1486
		4.23375	4.7745	0.2038
12	4	8.71588	1.317	0.26
		3.97408	8.6986	0.0537
		0.190801	43.8558	0.0289
		3.08217	19.985	0.0113
13	6	1.27577	31.5648	0.1212
		7.31592	2.6908	0.1223
		4.70793	8.9189	0.2072
		0.127577	60.684	0.1276
		4.80954	16.8861	0.1408
14	2	4.32407	14.3159	0.0795
		10.24003	3.4631	0.147
15	4	0.668368	33.3943	0.2549
		0.413214	54.8672	0.0807
		6.71755	11.2056	0.0835
		9.76585	2.7451	0.1494
16	5	3.43216	3.3553	0.007
		0.318378	43.964	0.281
		8.90781	6.6715	0.0418
		4.00795	0.9451	0.0866
		2.09994	15.6309	0.1973
17	4	0.445955	11.6028	0.0321
		4.516	1.0776	0.3688
		6.80787	4.1048	0.0366
		3.7257	25.335	0.1102
18	5	1.49028	33.8681	0.1854
		2.35961	1.1489	0.276
		4.83212	2.6644	0.1499
		0.254025	62.0229	0.4039
		8.39976	11.3276	0.0628
19	5	4.80954	15.4566	0.0886

		2.38219	1.0083	0.1699
		3.69183	6.9369	0.0807
		0.890781	35.4039	0.1177
		5.85951	3.1476	0.1365
20	5	4.9676	8.2526	0.1508
		0.859080938	27.18	0.1067
		0.0954005	48.4595	0.1985
		0.9862944	19.9805	0.2631
		8.94168	2.2393	0.2442
21	5	4.35794	10.6502	0.1628
		1.49028	20.708	0.1173
		5.50952	1.4027	0.2499
		6.2095	5.8868	0.0636
		0.827557	51.5237	0.3976
22	4	2.19026	16.7466	0.1126
		6.71755	6.9956	0.2205
		5.82564	1.8661	0.0178
		0.636756	33.8613	0.2659
23	3	7.57559	3.9571	0.0998
		0.127577	45.8298	0.2293
		4.00795	14.1292	0.1172
24	4	5.12566	1.7833	0.096
		6.04015	7.0394	0.1741
		2.44993	16.1833	0.0986
		1.49028	35.5546	0.0747
25	5	5.63371	5.0243	0.1911
		2.29187	31.4917	0.2784
		0.636756	56.9763	0.334
		6.61594	1.3932	0.4283
		4.00795	12.6347	0.2517
26	4	3.34184	20.6387	0.0427
		8.84007	2.4056	0.0755
		2.7096	8.9796	0.3064
		0.0318378	50.2494	0.3639
27	6	2.22413	2.5964	0.4219
		4.35794	0.7375	0.2903
		0.159189	45.0043	0.1013
		1.04997	27.0852	0.1127
		0.859169	14.592	0.3055
		7.66591	5.6235	0.0771
28	5	1.94188	30.3056	0.2623
		0.0318378	70.8099	0.1377

		5.15953	14.6722	0.2382
		4.83212	2.3172	0.1175
		3.46603	0.9207	0.0854
29	3	2.4838	34.9077	0.2854
		2.32574	19.4388	0.1095
		11.77547	3.2858	0.268
30	3	7.41753	10.7703	0.1094
		0.604015	44.4078	0.3727
		7.47398	1.4963	0.3857
31	5	4.93373	10.0401	0.2559
		1.49028	39.5564	0.3953
		2.64186	1.2422	0.206
		6.29982	3.1395	0.1274
		0.0318378	57.1226	0.4814
32	4	9.06587	12.2158	0.0948
		6.64981	2.833	0.0887
		2.32574	0.9159	0.1491
		0.636756	32.8533	0.0441
33	4	8.84007	1.6575	0.1485
		6.14176	8.6575	0.1244
		3.14991	24.3379	0.2215
		0.668368	50.9771	0.2573
34	6	1.62576	17.7691	0.2389
		0.34999	48.7852	0.1063
		6.58207	2.9664	0.0253
		2.76605	0.7744	0.172
		5.40791	11.0897	0.0516
		0.0318378	69.1131	0.1511
35	5	3.78215	1.2453	0.1904
		0.509179	36.3627	0.0847
		3.30797	15.4405	0.0926
		7.73365	5.74	0.1523
		0.0318378	84.3359	0.0589
36	3	0.69998	38.1482	0.5669
		9.29167	2.3079	0.1964
		6.74013	13.4875	0.119
37	4	6.55949	6.4703	0.1305
		1.20803	30.1744	0.3686
		6.84174	1.6763	0.138
		4.16601	13.5405	0.1514
38	4	3.40958	1.2514	0.4145
		6.07402	3.3952	0.0995

		2.83379	19.3795	0.2432
		4.35794	7.4497	0.0431
39	3	1.04997	0.4954	0.3193
		3.14991	18.2081	0.147
		10.84969	3.2193	0.1726
40	3	11.19968	2.6622	0.1265
		1.081582	44.9374	0.2079
		6.80787	16.6032	0.1832
41	4	9.86746	5.7068	0.0621
		2.67573	25.6636	0.1121
		4.16601	1.3489	0.3586
		0.0318378	67.6783	0.0687
42	3	6.93206	1.2212	0.211
		0.795945	25.6461	0.1143
		5.18211	9.4593	0.111
43	4	4.86599	5.5974	0.2127
		0.890781	40.0138	0.1843
		7.50785	1.7139	0.1184
		1.55802	9.8973	0.2734
44	4	6.68368	1.5705	0.0357
		3.08217	11.881	0.0229
		2.22413	35.033	0.464
		5.02405	7.2699	0.251
45	4	1.52415	19.0278	0.0999
		6.87561	1.6584	0.1793
		8.94168	7.2158	0.1898
		0.0318378	58.7253	0.476
46	6	0.509179	50.1471	0.127
		5.79177	3.4059	0.0821
		2.89024	8.4649	0.28
		0.827557	25.7252	0.1653
		5.02405	1.2636	0.0591
		0.0318378	76.5791	0.0382
47	6	4.2902	24.4238	0.0423
		6.26595	2.7315	0.1801
		5.5321	8.3866	0.0779
		3.53377	0.7508	0.251
		0.0318378	47.842	0.1484
		0.0318378	70.9679	0.3809
48	4	4.23375	12.9747	0.0529
		6.29982	1.1205	0.2409
		5.47565	6.0601	0.1348

		1.68221	29.8179	0.1263
49	4	4.93373	1.2726	0.2515
		0.286766	47.1495	0.4538
		3.14991	9.4572	0.1268
		6.64981	4.681	0.2314
50	5	7.82397	1.8337	0.0669
		4.00795	6.3048	0.0888
		0.540791	52.3614	0.1137
		0.890781	24.1444	0.1908
		4.516	11.5177	0.0114

Appendix 6:

The following table presents the results of the individual simulations with a surface mass density proportional to r^{-1} and a disk-to-mass ratio of .02.

Shallower				
#	Planet #	Mass	Radius	Eccentricity
1	4	0.95	40.6752	0.3082
		5.51	6.3485	0.07
		3.41	13.7147	0.0852
		4.39	1.9038	0.2346
2	5	4.97	2.5138	0.2043
		1.59	0.9739	0.1797
		6.77	6.7982	0.0872
		2.54	14.3779	0.1401
		0.13	50.6008	0.3818
3	3	9.19	2.3986	0.2404
		3.66	27.5781	0.283
		3.59	14.6881	0.04
4	4	5.06	9.0362	0.3261
		3.82	20.7074	0.1144
		7.42	2.8332	0.3066
		0.19	61.3035	0.3157
5	5	4.71	2.2778	0.3702
		4.04	7.0604	0.2391
		2.03	22.2488	0.1405
		0.06	57.4758	0.1694
		0.06	40.3771	0.4369
6	5	8.49	12.2233	0.1237
		0.79	25.3053	0.1947
		6.53	4.3771	0.1771
		0.10	52.2874	0.3749
		2.29	0.9472	0.1445
7	5	4.67	19.5345	0.1585
		7.63	2.532	0.3081
		1.05	34.9217	0.2486
		0.06	63.4479	0.0809
		0.99	9.0743	0.1146
8	4	0.19	63.589	0.0723
		5.22	7.8168	0.2254
		2.13	40.8033	0.2743
		8.47	2.4801	0.1349
9	5	7.47	4.3322	0.0679

		2.54	12.3463	0.1933
		0.25	52.9651	0.328
		3.88	1.6056	0.0629
		1.52	22.439	0.1584
10	4	8.05	4.2473	0.1764
		1.78	29.7657	0.2415
		3.12	9.2426	0.3162
		0.60	42.1719	0.1725
11	5	5.69	2.7415	0.338
		2.48	28.593	0.1793
		4.20	5.9968	0.4128
		3.94	14.9645	0.0983
		0.10	70.991	0.2335
12	4	4.67	21.2017	0.0763
		7.61	1.9857	0.0603
		1.28	50.9014	0.0961
		3.82	10.5891	0.1549
13	4	4.90	13.9128	0.1263
		7.89	2.6051	0.0743
		0.86	57.9223	0.3974
		2.52	6.3384	0.1285
14	4	1.84	40.8068	0.2296
		4.67	1.3978	0.3348
		12.25	7.5421	0.1007
		0.92	17.7897	0.3183
15	4	0.19	19.2346	0.295
		3.73	3.0739	0.0539
		2.83	39.1641	0.2975
		4.58	5.6177	0.1298
16	4	2.57	9.7772	0.0422
		0.29	53.9823	0.398
		9.48	3.2246	0.2129
		2.73	25.1649	0.1497
17	5	7.51	2.2374	0.0533
		6.37	11.0717	0.1546
		1.75	24.6633	0.166
		0.60	5.7506	0.114
		0.19	68.1503	0.2929
18	4	4.01	18.4782	0.183
		0.16	57.1892	0.2706
		0.92	8.9398	0.2833
		8.14	3.5709	0.0769

19	4	2.13	12.9865	0.2475
		0.67	52.2655	0.2423
		9.22	2.8859	0.1194
		3.12	19.8267	0.1028
20	5	3.38	1.6199	0.264
		2.19	20.6339	0.3533
		0.25	51.7406	0.0934
		4.13	3.7572	0.0824
		6.88	8.8397	0.0906
21	6	0.10	63.0056	0.2644
		4.27	9.0433	0.1275
		1.33	17.3496	0.099
		4.04	1.4063	0.281
		4.67	5.1586	0.0524
		2.61	29.9117	0.024
22	4	3.27	4.6147	0.1571
		1.87	29.4448	0.079
		7.12	10.8636	0.2897
		4.81	1.7168	0.1147
23	6	1.05	61.3582	0.1539
		7.32	8.0963	0.0917
		1.82	14.1307	0.0967
		3.62	2.5491	0.1926
		1.11	36.5932	0.3044
		2.57	0.7363	0.3577
24	4	1.31	15.0741	0.1143
		4.11	0.9232	0.2712
		2.92	30.8783	0.2132
		7.63	4.4974	0.3382
25	4	6.42	5.639	0.1813
		2.57	15.9217	0.0995
		1.11	34.1854	0.175
		5.51	2.236	0.1613
26	5	2.96	1.8503	0.4551
		1.52	15.2949	0.2248
		0.06	68.2264	0.174
		8.66	6.6384	0.0606
		1.08	45.9991	0.1869
27	3	0.32	66.9617	0.2221
		2.68	18.0715	0.2104
		11.39	3.7135	0.3469
28	4	0.19	48.2516	0.1282

		2.57	23.8558	0.2156
		4.62	11.7486	0.2031
		8.47	2.9221	0.1159
29	5	0.06	76.486	0.2471
		2.42	4.8011	0.1311
		7.58	2.4855	0.1186
		4.36	13.9339	0.1717
		2.99	28.7499	0.0241
30	5	2.96	19.1662	0.2097
		6.23	2.9338	0.101
		2.17	47.8294	0.4408
		3.69	7.3418	0.132
		2.13	1.1976	0.3746
31	4	3.03	20.5469	0.2283
		7.26	5.255	0.229
		5.34	1.377	0.2439
		0.03	55.4078	0.2742
32	3	2.99	24.8362	0.2954
		7.86	10.5307	0.1073
		7.51	2.4195	0.1623
33	4	0.70	31.4367	0.4103
		3.53	12.5577	0.0189
		9.19	2.128	0.365
		0.22	66.932	0.1368
34	4	2.87	17.7534	0.1854
		4.36	5.7332	0.1583
		1.17	49.7463	0.2444
		6.72	2.843	0.0829
35	5	3.78	1.3363	0.1317
		6.93	3.3506	0.049
		0.99	6.4472	0.026
		0.64	13.3521	0.1481
		3.24	23.7177	0.2078
36	3	4.46	2.1378	0.4808
		9.38	7.7694	0.2252
		2.96	38.7103	0.5916
37	4	4.58	25.198	0.1961
		8.28	3.9449	0.0528
		0.54	43.2479	0.3601
		1.87	0.8624	0.2558
38	5	9.48	8.1861	0.115
		2.03	29.267	0.1724

		2.42	1.0421	0.2056
		0.86	59.287	0.3342
		3.62	2.4568	0.3144
39	4	2.87	25.0598	0.116
		1.87	0.7784	0.268
		8.12	3.8687	0.1035
		2.83	11.7852	0.143
40	5	7.38	2.7913	0.1529
		0.13	54.2835	0.098
		3.85	5.9442	0.1041
		4.97	15.7478	0.0272
		1.02	35.9408	0.1145
41	3	7.54	2.9881	0.2037
		8.31	10.5477	0.1089
		1.56	52.7406	0.4646
42	5	0.57	44.123	0.0202
		5.63	10.0228	0.1963
		0.06	68.5425	0.151
		2.48	34.4431	0.0112
		7.96	2.4632	0.2245
43	4	5.51	7.2991	0.2412
		4.93	15.7355	0.2007
		7.07	2.3322	0.2723
		0.57	45.8181	0.1212
44	4	2.92	23.5672	0.2155
		4.27	10.9177	0.1366
		0.32	57.8321	0.1019
		8.08	3.196	0.0895
45	7	4.87	5.3551	0.0509
		4.27	2.8356	0.0652
		0.06	42.5844	0.092
		4.39	16.6879	0.0172
		0.06	56.4389	0.0861
		0.13	28.2913	0.0903
		1.21	0.6023	0.1061
46	5	5.88	2.2264	0.1462
		1.78	31.0662	0.1245
		5.44	5.901	0.1257
		5.48	11.8391	0.2346
		0.54	62.1259	0.3436
47	4	8.24	2.4038	0.3893
		3.38	23.7297	0.1158

		0.35	60.611	0.2701
		4.55	8.1071	0.2557
48	5	2.45	19.5696	0.1333
		0.06	57.7971	0.1318
		4.43	2.2255	0.083
		4.78	7.8352	0.0883
		2.89	0.9164	0.1624
49	4	3.73	6.0618	0.21
		0.80	37.1499	0.1718
		6.42	2.3789	0.1835
		7.00	14.1198	0.0815
50	4	5.60	13.0441	0.148
		8.65	2.4757	0.1508
		1.56	28.9371	0.2604
		2.61	6.1544	0.2051